

Anomalous Lattice Thermal Conductivity in Rocksalt IIA-VIA Compounds

S. C. Rakesh Roshan,^{*,†,‡} N. Yedukondalu,^{*,¶} Rajmohan Muthaiah,[§] K.
Lavanya,^{||,⊥} P. Anees,[#] R. Rakesh Kumar,[@] T. Venkatappa Rao,[@] Lars Ehm,[¶]
and John B. Parise[¶]

[†]*Rajiv Gandhi University of Knowledge Technologies, Basar, Telangana-504107, India*

[‡]*Department of Physics, National Institute of Technology-Warangal, Telangana, India*

[¶]*Department of Geosciences, Center for Materials by Design, and Institute for Advanced
Computational Science, State University of New York, Stony Brook, New York 11794-2100,
USA*

[§]*School of Aerospace and Mechanical Engineering, University of Oklahoma, Norman, OK
73019, USA*

^{||}*Jawaharlal Nehru Technological University (JNTU), Hyderabad, 500085, Telangana,
India.*

[⊥]*Telangana Social Welfare Residential Degree College for Women (TSWRDC-W),
Nizamabad, 503002, Telangana, India.*

[#]*Materials Physics Division, Indira Gandhi Centre for Atomic Research, Kalpakkam
603102, Tamil Nadu, India*

[@]*Department of Physics, Nanomaterials and Energy Harvesting Research Lab, National
Institute of Technology-Warangal, Telangana, India*

E-mail: roshan@rgukt.ac.in; nykondalu@gmail.com

Abstract

Materials with an intrinsic (ultra)low lattice thermal conductivity (k_L) are critically important for the development of efficient energy conversion devices. In the present work, we have investigated microscopic origins of low k_L behavior in BaO, BaS and MgTe by exploring lattice dynamics and phonon transport of 16 iso-structural MX (Mg, Ca, Sr, Ba and X = O, S, Se and Te) compounds in the rocksalt (NaCl)-type structure by comparing their lattice transport properties with the champion thermoelectric iso-structural material, PbTe. Anomalous trends are observed for k_L in MX compounds except the MgX series in contrast to the expected trend from their atomic mass. The underlying mechanisms for such low k_L behavior in relatively low atomic mass systems namely BaO, BaS and MgTe compounds are thoroughly analyzed. We propose the following dominant factors that might be responsible for low k_L behavior in these materials: 1) softening of transverse acoustic (TA) phonon modes despite low atomic mass, 2) low lying optic (LLO) phonon modes fall deep into acoustic mode region which enhances overlap between longitudinal acoustic (LA) and LLO phonon modes which increases scattering phase space, 3) short phonon lifetimes and high scattering rates, 4) relatively high density (ρ) and large Grüneisen parameter. Moreover, tensile strain also causes a further reduction in k_L for BaO, BaS and MgTe through phonon softening and near ferroelectric instability. Our comprehensive study on 16 binary MX compounds might provide a pathway for designing (ultra)low k_L materials even with simple crystal systems through phonon engineering.

Introduction

Discovery of materials with low lattice thermal conductivity gained tremendous interest due to their potential applications in thermoelectrics,¹⁻⁵ thermal barrier coatings,⁶⁻⁹ thermal insulation^{10,11} and thermal energy management.¹² Extensive efforts have been put forward by researchers in this direction to develop suitable materials for energy conversion applications during the last decade. Recently, binary alkaline-earth chalcogenides, MX (Mg, Ca, Sr, Ba and X = O, S, Se and Te) are being received considerable attention due to their potential applications in multifarious fields such as catalysis, microelectronics,¹³ optoelectronics (light emitting, laser and magneto optical devices)¹⁴⁻¹⁶ and thermoelectrics¹⁷⁻¹⁹ despite their simple crystal structure. Bulk MX & their 2D counterparts,¹⁷⁻²⁰ p-type PbTe & MTe nanocrystals,²¹ CaTe-SnTe,²² heavily doped SrTe with PbTe^{23,24} and BaTe-PbTe²⁵ are found to have excellent thermoelectric figure of merit (zT) in the range of 0.5-1.32.^{19,26} This shows the viability of these materials as power generating thermoelectric (TE) devices and are capable of converting waste heat into electricity. In general, the conversion efficiency is characterized by a dimensionless quantity *i.e.*, $zT = S\sigma^2T/k$, where $k = k_e + k_L$; S, σ , T are the Seebeck coefficient, electrical conductivity, and absolute temperature, and k_e and k_L are the electronic and lattice thermal conductivities, respectively. The complex interdependence among these S, σ and k parameters becomes challenging to discover the high zT materials. Therefore, materials with an intrinsic ultralow k (especially k_L) provide a pathway for discovering high zT materials without degrading its charge transport. The MX compounds are extensively studied from theoretical perspective, which mainly focused on exploring structural phase transitions,²⁷⁻³⁰ elastic,^{30,31} lattice dynamics,^{29,32-34} electronic structure,^{28,35-38} metallization,^{27,39-41} thermodynamic,^{42,43} thermoelectric properties¹⁷⁻¹⁹ at ambient and/or high pressure/temperature conditions. However, very limited studies have been dedicated towards understanding the phonon transport in MgSe,⁴⁴ MgTe,⁴⁵ CaX (X = O, S, Se and Te)⁴⁶ and MTe (M = Mg, Ca, Sr, Ba and Pb)⁴⁷ compounds. Therefore, a detailed and comparative study on phonon transport of MX compounds provide insights to

achieve (ultra)low k_L materials through phonon engineering, which is essential for discovery of high zT materials. In the present work, we shed more light on understanding lattice dynamics, phonon transport and mechanical properties of 16 MX compounds at ambient conditions. Interestingly, we observe anomalous trends in k_L for CaX (CaS > CaO > CaSe > CaTe), SrX (SrSe > SrO > SrS > SrTe) and BaX (BaTe > BaSe > BaS > BaO) series. Especially, the observed anomalous⁴⁸ trend in BaX (partly in SrX and CaX⁴⁶) series is in contrast to the expected trend from their atomic mass. Overall, among 16 compounds, we found BaO, BaS and MgTe exhibit low k_L behavior over the studied temperature range of 300-800 K despite their low atomic mass in rocksalt NaCl-type (B1) structure. The underlying mechanisms for such abnormal trends and low k_L behavior are extensively discussed through the computed lattice dynamics, phonon lifetimes, scattering rates, phonon group velocities at 300 K and mechanical properties. We also have investigated the effect of tensile strain on lattice dynamics and phonon transport of BaO, BaS and MgTe compounds are discussed extensively.

The rest of the paper is organized as follows: In the next section, we briefly describe the computational details, methodology, various parameters used to perform the computation and crystal structure. Results and discussions concerning anharmonic lattice dynamics, lattice thermal conductivity and mechanical properties of the 16 MX compounds. Finally, we propose important observations that will be helpful to achieve (ultra)low k_L in general and in particular for the MX compounds and finally summarized major outcomes of the present study.

Computational details, methodology and crystal structure

All the first principles calculations have been performed using Vienna Ab-initio Simulation Package (VASP)⁴⁹ for MX (Mg, Ca, Sr, Ba and X = O, S, Se and Te) compounds. The

exchange-correlation was treated with PBEsol functional and the electron-ion interactions with pseudo-potential based projected augmented wave (PAW) approach. We have considered 10 and 6 valence electrons for alkaline-earth metals (Mg, Ca, Sr and Ba) and chalcogens (O, S, Se and Te) as plane wave basis orbitals. A plane wave cutoff energy of 520 eV was used for plane wave basis set expansion and a spacing of $2\pi \times 0.024 \text{ \AA}^{-1}$ for k-mesh in the irreducible Brillouin zone. Since MX compounds are polar semiconductors, Born effective charges and dielectric constants are calculated using density functional perturbation theory to capture dipole-dipole interactions.

Lattice dynamics and thermal conductivity of MX compounds are calculated by considering harmonic (2^{nd}) and anharmonic (3^{rd}) inter atomic force constants (IFCs) using the temperature dependent effective potential (TDEP)⁵⁰⁻⁵² method. In the present work, we have considered the expansion of inter atomic force constants (IFCs) up to 3^{rd} order and the corresponding model Hamiltonian is given as follows:

$$H = U_0 + \sum_i \frac{p_i^2}{2m_i} + \frac{1}{2!} \sum_{ij} \sum_{\alpha\beta} \Phi_{ij}^{\alpha\beta} u_i^\alpha u_j^\beta + \frac{1}{3!} \sum_{ijk} \sum_{\alpha\beta\gamma} \psi_{ijk}^{\alpha\beta\gamma} u_i^\alpha u_j^\beta u_k^\gamma \quad (1)$$

where p_i and u_i are momentum and displacement of atom i , respectively. $\Phi_{ij}^{\alpha\beta}$ and $\psi_{ijk}^{\alpha\beta\gamma}$ are 2^{nd} and 3^{rd} order force constant matrices, respectively. To compute these harmonic (2^{nd}) and anharmonic (3^{rd}) inter atomic force constants (IFCs), we have performed ab initio molecular dynamics (AIMD) simulations as implemented in the VASP at 300 K. The AIMD calculations were run for 5000 MD steps with time-step of 1 fs (*i.e.*, 5 ps) with 128 atoms ($4 \times 4 \times 4$) supercell for all the MX compounds. For 2^{nd} and 3^{rd} order IFCs, interactions up to 9^{th} nearest neighbors were included to ensure the convergence of calculated lattice dynamics and phonon transport properties. The temperature was controlled with a Nosé-Hoover thermostat.^{53,54} The lattice thermal conductivity is calculated by iteratively solving the full Boltzmann transport equation (BTE), including three-phonon and isotope scatterings from the natural distribution on a $25 \times 25 \times 25$ q-point grid.

The thermal conductivity tensor is given by

$$k^{\alpha\beta} = \frac{1}{(2\pi)^3} \sum_s \int dq C_\lambda v_{\lambda\alpha} v_{\lambda\beta} \tau_{\lambda\beta} \quad (2)$$

where C_λ is the contribution per mode $\lambda = (s, q)$ to specific heat, α and β are Cartesian components, v_β and τ_β are phonon velocity and scattering time, respectively.

The scattering rates are calculated from a full inelastic phonon Boltzmann equation which is given by

$$k_B T v_\lambda \cdot \nabla T \frac{\partial n_{0\lambda}}{\partial T} = \sum_{\lambda'\lambda''} \left[P_{\lambda\lambda'\lambda''}^+ (\Psi_{\lambda''} - \Psi_{\lambda'} - \Psi_\lambda) + \frac{1}{2} P_{\lambda\lambda'\lambda''}^- (\Psi_{\lambda''} + \Psi_{\lambda'} - \Psi_\lambda) \right] \quad (3)$$

The left-hand side represents the phonon diffusion induced by the thermal gradient ∇T and $n_{0\lambda}$ is the equilibrium phonon distribution function. While the right-hand side corresponds to the collision term for three-phonon interactions. v_λ is the phonon velocity in mode λ , $P_{\lambda\lambda'\lambda''}^+$ and $P_{\lambda\lambda'\lambda''}^-$ are three phonon scattering rates for absorption ($\lambda + \lambda' \rightarrow \lambda''$) and emission ($\lambda \rightarrow \lambda' + \lambda''$) processes, respectively.

Binary alkaline-earth chalcogenides, MX (Mg, Ca, Sr, Ba and X = O, S, Se and Te) compounds except MgSe and MgTe crystallize in the face centred cubic (FCC) rocksalt NaCl (B1)-type structure (see Figure 1) having space group $Fm\bar{3}m$ with $Z = 4$ formula units (f.u.) per unit cell at ambient conditions.⁵⁵⁻⁶¹ MgSe and MgTe exhibit rich polymorphism and they crystallize in rocksalt (B1), zinc-blende (B3), wurtzite (B4) and NiAs (B8)-type structures. The X-ray diffraction measurements reveal that MgTe crystallizes in B3⁶² and B8⁶³ structures at ambient conditions. First principles calculations disclose that B3³⁸ phase for MgSe and both B3³⁸ and B8⁶⁴⁻⁶⁶ for MgTe are thermodynamically stable structures at ambient conditions. Moreover, rocksalt-type B1 structure is dynamically stable (meta-stable) for both MgSe and MgTe compounds. Therefore, in the present work, we have considered B1 structure for all the MX compounds which allow us for direct comparison of the calculated properties among these 16 systems under investigation. Table 1 presents the calculated

ground state equilibrium lattice constant for MX compounds in comparison with reported X-ray diffraction measurements^{55–60,67–70} and previous first principles calculations^{17,19,38,71–78} and there is a good agreement among them. In addition, we also calculated the electron localization function (ELF) for MgO, BaO, MgTe and PbTe compounds. As shown in Figure 1, the metal cations (Mg^{2+} , Ba^{2+}) donate the electrons while anions (O^{2-} , Te^{2-}) gains the electrons indicating complete transfer of charge thus resulting in strong ionic bonding which is consistent with the fact that large electronegativity difference between Mg (1.31 in Pauling scale), Ba (0.89) and O (3.44) results in strong ionic character for MgO (2.13) and BaO (2.55). The low electronegativity difference (0.79) between Mg (1.31) and Te (2.10) atoms suggest a polar covalent bonding along with ionic bonding in MgTe, while lone-pair of $6s^2$ valence electrons is observed for PbTe along with sharing of electrons between Pb and Te. The distinct chemical bonding nature strongly influences k_L of these materials.

Results and Discussion

Anharmonic lattice dynamics and thermal conductivity

Exploring lattice dynamics including anharmonic effects is crucial for understanding phonon transport in materials. As a first step, we have computed phonon dispersion curves (Figure 2) of MX compounds at 300 K and thoroughly analyzed them. As shown in Figure 2, no imaginary frequencies are found along high symmetry directions of the Brillouin zone indicating that all the investigated materials are dynamically stable. MX materials consist of 2 atoms per primitive cell resulting in $(3N; N = \text{number of atoms per primitive cell})$ 6 vibrational modes of which 3 are acoustic and 3 are optic modes. Dipole-dipole interactions are crucial for polar materials to describe phonon spectra correctly. These interactions are incorporated into dynamical matrix through calculated Born effective charges and high frequency dielectric constants which in turn produces a splitting between longitudinal optic (LO) and transverse optic (TO) phonon modes (Figure 2). Due to this LO-TO splitting, the

three phonon optic modes split into two degenerate TO (ω_{TO}) and one LO (ω_{LO}) modes along Γ -direction. Large LO-TO splitting is observed in particular for MO compounds and it is increasing from MgO < CaO < SrO < BaO, while it is decreasing from MO > MS > MSe > MTe compounds (see Figure 2 & Table S1). The MX compounds exhibit similar phonon band features and showed a significant phonon softening with increasing atomic mass from Mg \rightarrow Ca \rightarrow Sr \rightarrow Ba and O \rightarrow S \rightarrow Se \rightarrow Te and these features are consistent with previous first principles lattice dynamical calculations.^{17-19,47} The calculated lattice thermal conductivity (k_L) as function of temperature (300-800 K) is presented in Figure 3, the calculated k_L values are decreasing with temperature for all the 16 compounds under investigation. Usually, materials with same crystal structure that consist of heavy elements, possess low k_L compared to the ones with light elements due to their high atomic mass. As expected, k_L is decreasing with increasing atomic mass of anion *i.e.*, from MgO \rightarrow MgS \rightarrow MgSe \rightarrow MgTe in MgX compounds, while k_L shows anomalous trends for CaX (CaS > CaO > CaSe > CaTe), SrX (SrSe > SrO > SrS > SrTe) and BaX (BaTe > BaSe > BaS > BaO) series of compounds. Especially, BaX series shows an opposite trend for k_L in contrary to the expected trend from their atomic masses. However, the above trends are slightly altered, when k_L is computed at the experimental lattice constant for SrX (SrSe > SrO \geq SrS > SrTe) and BaX (BaSe \geq BaTe > BaO > BaS) compounds but the overall trends remain more or less similar in both the cases (see Figures 3 & S2). Usually, the PBE-GGA functional overestimates equilibrium lattice constant, therefore, the obtained k_L values are underestimated when compared to the experimental values.⁴⁶ Since, PBEsol functional underestimated the equilibrium lattice constant for PbTe (see Table 1), the obtained k_L values are overestimated compared to the ones obtained at the experimental lattice constant over the studied temperature range and this clearly demonstrates sensitivity of k_L towards lattice constant(s) (see Figure S3). The predicted anomalous trends are originated from phonon softening observed from phonon dispersion curves (see Figure 2). As shown in Figure 2c & d, low lying TO modes of MO (M = Ca, Sr and Ba), SrS and BaS compounds fall deep into acoustic mode region in general

and in particular for BaO¹⁹ and SrO¹⁹ compounds (see Figure 2) as observed for heavy metal binary PbTe.⁴⁷ This enhances the overlap between TO and acoustic phonon modes which increases the scattering phase space, thus resulting in reduction of k_L in those compounds. In addition, BaO shows extra phonon softening of acoustic modes near L point in the first Brillouin zone despite its low atomic mass compared to the rest of BaX (X = S, Se and Te) compounds. Among the 16 systems under investigation, interestingly, three compounds namely BaO, BaS and MgTe exhibit low k_L *i.e.*, below $\sim 6 \text{ Wm}^{-1}\text{K}^{-1}$ at 300 K. MgTe shows relatively low k_L because of soft acoustic phonon modes near X and L points in the first Brillouin zone despite its low atomic mass compared to the rest of MTe (M = Ca, Sr, and Ba) compounds. This trend is consistent with the previous compressive sensing lattice dynamics (CSLD) study⁴⁷ but in contrast to the phenomenological Debye-Callaway model study⁷⁹ on lattice thermal transport of MTe (M = Mg, Sr, Ba and Pb) compounds. In addition, the k_L values are severely underestimated using Debye-Callaway model (see Table 2). Overall, we observed two important aspects from phonon dispersion curves, which might be responsible for low k_L behavior in BaO, BaS and MgTe compounds: 1) low lying TO phonon modes fall deep into acoustic mode region for BaO and BaS, 2) soft acoustic (TA) phonon modes of MgTe despite its low atomic mass over other heavy metal MTe (M = Ca, Sr, Ba) tellurides.

To further explore the underlying mechanisms which are responsible for the observed anomalous behavior of k_L in MgTe, CaX, SrX and BaX compounds (see Figures 3, S1 and S2), we have calculated phonon mean free paths (MFPs), phonon lifetimes, group velocities and scattering rates. The calculated phonon MFPs as a function of frequency are presented in Figure S4. For all the MX compounds, a large portion of the phonon MFPs fall above the minimum inter-atomic distance or so called Ioffe-Regel limit. Therefore, phonon Boltzmann transport theory is good enough to describe thermal transport in MX compounds. In crystalline materials, the heat transport can be understood as the propagation of phonons and their scatterings among themselves. Since $k_L \propto \tau(\omega)$ and $v(\omega)$, therefore, materials with low

$\tau(\omega)$ and $v(\omega)$ expected to have low k_L .

As illustrated in Figure 4, phonon lifetime decreases from $\text{MgO} > \text{MgS} > \text{MgSe} > \text{MgTe}$ over the entire frequency range and the same trend is followed for k_L in MgX . While CaO has relatively shorter phonon lifetimes than CaS in the frequency range of $\sim 2\text{-}8$ THz (see Figure 4b), which might be reason for low k_L of CaO thus results in the anomalous trend ($\text{CaS} > \text{CaO} > \text{CaSe} > \text{CaTe}$) for k_L in CaX series. This trend is consistent with the previous lattice thermal conductivity study⁴⁶ on CaX compounds using ShengBTE. SrSe and SrO possess relatively highest and shorter phonon lifetimes in the frequency range of $\sim 1\text{-}4$ THz and $\sim 2\text{-}4$ THz, respectively. This could be a possible reason for the anomalous trend ($\text{SrSe} > \text{SrO} > \text{SrS} > \text{SrTe}$) observed in SrX series for k_L . Finally, BaO and BaS have the shortest phonon lifetimes over BaSe and BaTe in turn they have low k_L and this is consistent with the trend $\text{BaTe} > \text{BaSe} > \text{BaS} > \text{BaO}$ predicted for k_L in BaX compounds.⁴⁸

As shown in Figure S5, total scattering rates are obtained through summation of absorption, emission and isotope scattering rates from the three phonon processes for all the 16 MX compounds. The absorption scattering rates are largely dominated in the low frequency region (for instance, below 3 THz for BaO). In the low frequency region, phonon scattering processes probably occur through conversion of low energy phonon to a high energy phonon with an absorption of a phonon. The contribution of emission scattering rates gradually increase with frequency and are largely dominated at high frequency region, where phonon scattering processes probably occur through conversion of high energy phonon to a low energy phonon with an emission of a phonon. Finally, a moderate contribution from isotope scattering rates are observed over the entire frequency range, for instance, BaX compounds (see Figure S5).

Effect of tensile strain on lattice thermal conductivity

Out of 16 MX compounds, three of them (BaO , BaS and MgTe) found to have low k_L ($< 6 \text{ Wm}^{-1}\text{K}^{-1}$) over the studied temperature range of 300-800 K. As illustrated in Figure 5,

we compared phonon dispersion curves, phonon lifetimes, scattering rates and k_L of BaO, BaS and MgTe compounds with PbTe. Softening of acoustic modes due to its high atomic mass (see Figure 5a), high scattering rates (see Figure 5b) and short phonon lifetimes (see Figure 5c) of PbTe responsible for its low k_L behavior over BaO, BaS and MgTe compounds. The obtained k_L values follow exactly the decreasing order of phonon lifetimes for these four compounds, which is given as follows: BaS > BaO > MgTe > PbTe (see Figure 5c & d). Based on this trend and observed trends for other MX compounds (see Figure 4) clearly show that phonon lifetime (τ) is a dominating factor to determine k_L behavior in iso-structural compounds with the same crystal symmetry.

We then considered these three BaO, BaS and MgTe compounds to investigate the effect of tensile strain on lattice dynamics and phonon transport. Further to lower k_L , we applied tensile strain, which is an effective strategy to achieve (ultra)low k_L in materials. We have systematically increased the obtained equilibrium lattice constant up to 6% but we observed soft phonon modes with tensile strain $\geq 5\%$ of the equilibrium lattice constant for BaO, therefore, we studied the effect of tensile strain up to 4% for these three compounds. As illustrated in Figures 6a, 7a & 8a, with increasing strain, acoustic and TO phonon modes are getting softened, which increases the coupling strength between acoustic and TO phonon modes. This eventually increases phonon-phonon scattering rates with increasing strain (see Figure 6b, 7b, 8b), which causes a reduction in k_L over the studied temperature range. The phonon lifetime decreases (see Figure 6c, 7c, 8c) significantly due to high scattering rates for both acoustic and low lying TO modes with increase in tensile strain which is responsible for further lowering of k_L (see Figure 6d, 7d, 8d). The obtained k_L values for 4% of tensile strain at 300 K are ~ 2.06 , ~ 2.38 , $\sim 1.05 \text{ Wm}^{-1}\text{K}^{-1}$ for BaO, BaS and MgTe, respectively. The (ultra)low k_L of strained MgTe might be a better candidate for energy conversion applications. From the present and previous studies,⁴⁶ one can expect a similar behavior for other MX compounds with application of tensile strain.

Elastic constants and mechanical properties

To explore inter atomic bonding strength, lattice anharmonicity and mechanical stability of MX compounds, we have calculated second order elastic constants (C_{ij}). Since all the studied MX compounds crystallize in the cubic ($Fm\bar{3}m$) structure, they have three independent elastic constants such as longitudinal (C_{11}), transverse (C_{12}) and shear (C_{44}) due to symmetry constraints ($C_{11} = C_{22} = C_{33}$, $C_{12} = C_{13} = C_{23}$, $C_{44} = C_{55} = C_{66}$ and $C_{ij} = C_{ji}$). The calculated second order elastic constants are given in Table S2 and are consistent with the available ultrasonic pulse echo⁸⁰⁻⁸² and Brillouin scattering measurements⁸³ as well as with previous first principles calculations.^{19,42,78,79,84-88} The obtained elastic constants satisfy the Born stability criteria^{89,90} indicating the mechanical stability of all these MX compounds.

$$C_{11} - C_{12} > 0, C_{11} > 0, C_{44} > 0, C_{11} + 2C_{12} > 0 \quad (4)$$

We then computed bulk (B) and shear (G) moduli from the calculated elastic constants with Voigt-Reuss-Hill (VRH) approximation using equations 5 and 6, respectively. Later, B and G values are used to calculate Young's modulus (E) using equation 7. Since MgO has the highest E value, it is the stiffest material among the 16 MX compounds.

$$B = \frac{C_{11} + 2C_{12}}{3} \quad (5)$$

$$G = \frac{1}{2} \left[\frac{C_{11} - C_{12} + 3C_{44}}{5} + \frac{5C_{44}(C_{11} - C_{12})}{4C_{44} + 3(C_{11} - C_{12})} \right] \quad (6)$$

$$E = \frac{9BG}{3B + G} \quad (7)$$

The calculated C_{ij} 's, E, B, G moduli decrease from MO to MTe (M = Mg, Ca, Sr, Ba), which indicates the weak electrostatic/interatomic interactions in the lattice with increase in atomic size *i.e.*, from Mg to Ba and O to Te. Therefore, the materials with higher atomic size can be easily deformed under mechanical stress thus results in low elastic moduli or soft

lattice for systems with higher atomic mass.

$$\sigma = \frac{3B - 2G}{2(3B + G)} \quad (8)$$

$$\gamma_\sigma = \frac{3}{2} \left(\frac{1 + \sigma}{2 - 3\sigma} \right) \quad (9)$$

The typical values of Poisson's ratio (σ) are 0.1 and 0.25 for covalent and ionic materials, respectively.⁹¹ The obtained σ values span in the range of 0.18-0.28, which infer a strong ionic contribution in the interatomic bonding for these MX compounds (see Figure 1). MgO (0.18) and BaO (0.28) have the smallest and largest σ values, respectively among all the 16 MX compounds. The obtained σ value 0.28 for BaO is close to the σ of 0.25 (0.28⁹²) for PbTe. Further, the σ values are used to calculate the Grüneisen parameter (γ_σ).

Strength of lattice anharmonicity of a material is represented by Grüneisen parameter (γ_ω) which is usually obtained from phonons. However, computation of γ_ω involves a series of expensive phonon calculations and repeating them for 16 compounds is computationally demanding. To avoid this, we have used an efficient formula to compute γ_σ using Poisson's ratio (σ).⁹³ The obtained γ_σ using equation 9 for materials with RS structure is in excellent agreement with γ_ω .^{92,94} Since the 16 materials under investigation crystallize in B1, we have used equation 9 to compute γ_σ based on obtained σ values with equation 8. Also, the obtained γ_σ value 1.63 for BaO is closely comparable with γ_σ 1.50 (1.65⁹²) for PbTe. The deviation between this work and previous⁹² studies might be due to distinct lattice constant used for computation of elastic constants, which are highly sensitive to the lattice constant used in the calculations. As shown in Figure 9, BaO has the highest γ_σ , which indicates relatively high anharmonicity of BaO over other MX compounds which in turn leads to low k_L . We then calculated sound velocities (v_l , v_t , v_m) and Debye temperature (Θ_D) using the following relationships:

$$v_l = \sqrt{\frac{B + \frac{4G}{3}}{\rho}} \quad (10)$$

$$v_t = \sqrt{\frac{G}{\rho}} \quad (11)$$

$$v_m = \left[\frac{1}{3} \left(\frac{1}{v_l^3} \right) + \left(\frac{2}{v_t^3} \right) \right]^{-\frac{1}{3}} \quad (12)$$

$$\Theta_D = \frac{h}{k_B} \left[\left(\frac{3N}{4\pi V} \right) \right]^{\frac{1}{3}} v_m \quad (13)$$

Here, ρ , h , k_B , N and V are the crystal density, Planck constant, Boltzmann constant, and number of atoms and volume of unit cell.

The calculated v_l , v_t , v_m and Θ_D are decreasing from MO to MTe ($M = \text{Mg, Ca, Sr, Ba}$). Figures 10 and S7 show the variation of k_L as a function of Debye temperature (Θ_D), average (v_m), and longitudinal (v_l), transverse (v_t) sound velocities for the 16 MX compounds. The same trend is observed for all these four properties v_l , v_t , v_m and Θ_D . According to the Slack theory, low θ_D are indicative of low k_L in materials. In fact, the presence of LLO phonons results in a softening of the acoustic phonon modes, which yields low group velocities and frequencies for acoustic phonons, thus results in low θ_D . However, BaO, BaS and MgTe compounds have low k_L despite their higher v_l , v_t , v_m and Θ_D over other MTe ($M = \text{Ca, Sr, Ba}$), BaSe, SrSe compounds. Moreover, the calculated phonon group velocities for BaX compounds (see Figure S8) also follow their atomic mass trend consistent with sound velocities. This results strongly suggest that phonon lifetime is the dominant factor over group velocity which is mainly responsible for the observed anomalous trends in MX compounds along with LLO and low frequency acoustic modes.

Conclusions

In summary, we have systematically investigated lattice dynamics, phonon transport and mechanical properties of 16 binary systems with rocksalt-type structure and compared their properties with an efficient thermometric material, PbTe. We predicted anomalous trends for k_L in CaX ($\text{CaS} > \text{CaO} > \text{CaSe} > \text{CaTe}$), SrX ($\text{SrSe} > \text{SrO} > \text{SrS} > \text{SrTe}$) and BaX ($\text{BaTe} >$

BaSe > BaS > BaO) series of compounds. In particular, we observed an opposite trend for k_L in BaX series which is in contrast to the expected trend from their atomic masses. However, the above trends are slightly altered for SrX and BaX compounds, when k_L is computed at the experimental lattice constant. The possible reasons for such low k_L behavior in BaO, BaS and MgTe compounds might be due to the following: 1) softening of acoustic (TA) phonon modes despite of low atomic mass 2) low lying TO phonon modes fall deep into acoustic mode region which enhances phonon scattering phase space, 3) short phonon lifetimes and high scattering rates, 4) high density (ρ) and large Grüneisen parameter (γ_σ). Application of tensile strain further reduces k_L in BaO, BaS and MgTe through phonon softening which increases scattering rates thereby lowering phonon lifetimes. Overall, the present study provides insights to achieve (ultra)low k_L materials through phonon engineering in simple crystal systems, which is essential for the development of sustainable energy conversion devices for future energy applications.

Acknowledgments

SCR and NYK contributed equally to the manuscript. SCR would like thank RGUKT Basar for providing computational facilities. NYK would like to thank Prof. Olle Hellman, Linköping University, Sweden for his valuable suggestions. NYK also would like to thank Science and Engineering Research Board and Indo-US Scientific Technology Forum for providing financial support through SERB Indo-US postdoctoral fellowship and Stony Brook Research Computing and Cyberinfrastructure, and the Institute for Advanced Computational Science at Stony Brook University for access to the high-performance SeaWulf computing system, which was made possible by a \$1.4M National Science Foundation grant (#1531492).

References

- (1) Lin, W.; He, J.; Su, X.; Zhang, X.; Xia, Y.; Bailey, T. P.; Stoumpos, C. C.; Tan, G.; Rettie, A. J. E.; Chung, D. Y. et al. Ultralow Thermal Conductivity, Multiband Electronic Structure and High Thermoelectric Figure of Merit in TlCuSe . *Advanced Materials* **2021**, *n/a*, 2104908.
- (2) Cai, S.; Hao, S.; Luo, Y.; Su, X.; Luo, Z.-Z.; Hu, X.; Wolverton, C.; Dravid, V. P.; Kanatzidis, M. G. Ultralow Thermal Conductivity and Thermoelectric Properties of $\text{Rb}_2\text{Bi}_8\text{Se}_{13}$. *Chemistry of Materials* **2020**, *32*, 3561–3569.
- (3) Hu, L.; Fang, Y.-W.; Qin, F.; Cao, X.; Zhao, X.; Luo, Y.; Repaka, D. V. M.; Luo, W.; Suwardi, A.; Soldi, T. et al. High thermoelectric performance enabled by convergence of nested conduction bands in $\text{Pb}_7\text{Bi}_4\text{Se}_{13}$ with low thermal conductivity. *Nature Communications* **2021**, *12*, 4793.
- (4) Ding, J.; Lanigan-Atkins, T.; Calderón-Cueva, M.; Banerjee, A.; Abernathy, D. L.; Said, A.; Zevalkink, A.; Delaire, O. Soft anharmonic phonons and ultralow thermal conductivity in $\text{Mg}_3(\text{Sb}, \text{Bi})_2$ thermoelectrics. *Science Advances* **2021**, *7*, eabg1449.
- (5) Dutta, M.; Sarkar, D.; Biswas, K. Intrinsically ultralow thermal conductive inorganic solids for high thermoelectric performance. *Chem. Commun.* **2021**, *57*, 4751–4767.
- (6) Liu, B.; Zhao, J.; Liu, Y.; Xi, J.; Li, Q.; Xiang, H.; Zhou, Y. Application of high-throughput first-principles calculations in ceramic innovation. *Journal of Materials Science & Technology* **2021**, *88*, 143–157.
- (7) Clarke, D. R.; Phillpot, S. R. Thermal barrier coating materials. *Materials Today* **2005**, *8*, 22–29.
- (8) Liu, B.; Liu, Y.; Zhu, C.; Xiang, H.; Chen, H.; Sun, L.; Gao, Y.; Zhou, Y. Advances on

- strategies for searching for next generation thermal barrier coating materials. *Journal of Materials Science & Technology* **2019**, *35*, 833–851.
- (9) Zhang, J.; Guo, X.; Jung, Y.-G.; Li, L.; Knapp, J. Lanthanum zirconate based thermal barrier coatings: A review. *Surface and Coatings Technology* **2017**, *323*, 18–29, Advanced Coatings for Energy and Environmental Applications – Design, Processing, Properties, and Performance.
- (10) Bsaibess, E.; Delorme, F.; Monot-Laffez, I.; Giovannelli, F. Ultra-low thermal conductivity in scheelite and A-deficient scheelite ceramics. *Scripta Materialia* **2021**, *201*, 113950.
- (11) Liu, Y.; Jia, D.; Zhou, Y.; Zhou, Y.; Zhao, J.; Li, Q.; Liu, B. Discovery of ABO_4 scheelites with the extra low thermal conductivity through high-throughput calculations. *Journal of Materiomics* **2020**, *6*, 702–711.
- (12) Gibson, Q. D.; Zhao, T.; Daniels, L. M.; Walker, H. C.; Daou, R.; Hébert, S.; Zanella, M.; Dyer, M. S.; Claridge, J. B.; Slater, B. et al. Low thermal conductivity in a modular inorganic material with bonding anisotropy and mismatch. *Science* **2021**, *373*, 1017–1022.
- (13) Zimmer, H. G.; Winzen, H.; Syassen, K. High-pressure phase transitions in CaTe and SrTe. *Phys. Rev. B* **1985**, *32*, 4066–4070.
- (14) Pandey, R.; Sivaraman, S. Spectroscopic properties of defects in alkaline-earth sulfides. *Journal of Physics and Chemistry of Solids* **1991**, *52*, 211 – 225.
- (15) Asano, S.; Yamashita, N.; Nakao, Y. Luminescence of the Pb^{2+-} Ion Dimer Center in CaS and CaSe Phosphors. *physica status solidi (b)* **1978**, *89*, 663–673.
- (16) Nakanishi, Y.; Ito, T.; Hatanaka, Y.; Shimaoka, G. Preparation and luminescent properties of SrSe:Ce thin films. *Applied Surface Science* **1993**, *65-66*, 515 – 519.

- (17) Rajput, K.; Roy, D. R. h-CaS and h-CaSe nanosheets in CaX (X=O, S, Se and Te) series: promising thermoelectric materials under DFT investigation. *Applied Nanoscience* **2019**, *9*, 1845–1856.
- (18) Rajput, K.; Roy, D. R. Structure, stability, electronic and thermoelectric properties of strontium chalcogenides. *Physica E: Low-dimensional Systems and Nanostructures* **2020**, *119*, 113965.
- (19) Kumar, P.; Rajput, K.; Roy, D. R. Structural, electronic, vibrational, mechanical and thermoelectric properties of 2D and bulk BaX (X=O, S, Se and Te) series under DFT and BTE framework. *Physica E: Low-dimensional Systems and Nanostructures* **2021**, *127*, 114523.
- (20) Zheng, H.; Li, X.-B.; Chen, N.-K.; Xie, S.-Y.; Tian, W. Q.; Chen, Y.; Xia, H.; Zhang, S. B.; Sun, H.-B. Monolayer II-VI semiconductors: A first-principles prediction. *Phys. Rev. B* **2015**, *92*, 115307.
- (21) Biswas, K.; He, J.; Wang, G.; Lo, S.-H.; Uher, C.; Dravid, V. P.; Kanatzidis, M. G. High thermoelectric figure of merit in nanostructured p-type PbTe–MTe (M = Ca, Ba). *Energy Environ. Sci.* **2011**, *4*, 4675–4684.
- (22) Al Rahal Al Orabi, R.; Mecholsky, N. A.; Hwang, J.; Kim, W.; Rhyee, J.-S.; Wee, D.; Fornari, M. Band Degeneracy, Low Thermal Conductivity, and High Thermoelectric Figure of Merit in SnTe–CaTe Alloys. *Chemistry of Materials* **2016**, *28*, 376–384.
- (23) Tan, G.; Shi, F.; Hao, S.; Zhao, L.-D.; Chi, H.; Zhang, X.; Uher, C.; Wolverton, C.; Dravid, V. P.; Kanatzidis, M. G. Non-equilibrium processing leads to record high thermoelectric figure of merit in PbTe–SrTe. *Nature Communications* **2016**, *7*, 12167.
- (24) Kim, Y.-J.; Zhao, L.-D.; Kanatzidis, M. G.; Seidman, D. N. Analysis of Nanoprecipitates in a Na-Doped PbTe–SrTe Thermoelectric Material with a High Figure of Merit. *ACS Applied Materials & Interfaces* **2017**, *9*, 21791–21797, PMID: 28590114.

- (25) Lo, S.-H.; He, J.; Biswas, K.; Kanatzidis, M. G.; Dravid, V. P. Phonon Scattering and Thermal Conductivity in p-Type Nanostructured PbTe-BaTe Bulk Thermoelectric Materials. *Advanced Functional Materials* **2012**, *22*, 5175–5184.
- (26) Fan, T.; Oganov, A. R. Discovery of high performance thermoelectric chalcogenides through first-principles high-throughput screening. *J. Mater. Chem. C* **2021**, *9*, 13226–13235.
- (27) Pozhivatenko, V. Ionic Character, Phase Transitions, and Metallization in Alkaline-Earth Metal Oxides and Chalcogenides under Pressure. *Ukrainian Journal of Physics* **2020**, *65*, 1022.
- (28) Zagorac, D.; Doll, K.; Zagorac, J.; Jordanov, D.; Matović, B. Barium Sulfide under Pressure: Discovery of Metastable Polymorphs and Investigation of Electronic Properties on ab Initio Level. *Inorganic Chemistry* **2017**, *56*, 10644–10654, PMID: 28836771.
- (29) Bayrakci, M.; Colakoglu, K.; Deligoz, E.; Ciftci, Y. O. A first-principle study of the structural and lattice dynamical properties of CaX (X=S, Se, and Te). *High Pressure Research* **2009**, *29*, 187–203.
- (30) Hao, A. M.; Yang, X. C.; Gao, Z. M.; Liu, X.; Zhu, Y.; Liu, R. P. First-principles investigations on structural and elastic properties of CaX (X=S, Se and Te) under high pressure. *High Pressure Research* **2010**, *30*, 310–317.
- (31) Abdus Salam, M. M. Theoretical study of CaO, CaS and CaSe via first-principles calculations. *Results in Physics* **2018**, *10*, 934–945.
- (32) Şule Uğur, Theoretical study of the phonon properties of SrS. *Materials Science and Engineering: B* **2009**, *162*, 116–119.
- (33) Rakesh Roshan, S.; Kunduru, L.; Yedukondalu, N.; Sainath, M. Structure and Lattice

- Dynamics of Calcium Chalcogenides under High Pressure. *Materials Today: Proceedings* **2018**, *5*, 18874–18878.
- (34) Zhang, X.-D.; Li, Z.-J.; Shi, G.-M. Lattice Dynamics Study of Magnesium Chalcogenides. *Communications in Theoretical Physics* **2012**, *57*, 295–300.
- (35) Lv, T.; Chen, D.; Huang, M. Quasiparticle band structures of BaO and BaS. *Journal of Applied Physics* **2006**, *100*, 086103.
- (36) Sajjad, M.; Zhang, H. X.; Noor, N. A.; Alay-e Abbas, S. M.; Younas, M.; Abid, M.; Shaukat, A. Theoretical Investigation of Structural, Electronic, and Magnetic Properties of V-Doped MgSe and MgTe Semiconductors. *Journal of Superconductivity and Novel Magnetism* **2014**, *27*, 2327–2336.
- (37) Yedukondalu, N.; Kunduru, L.; Roshan, S. C. R.; Sainath, M. Assessment of band gaps for alkaline-earth chalcogenides using improved Tran Blaha-modified Becke Johnson potential. *AIP Conference Proceedings* **2018**, *1942*, 090030.
- (38) Tairi, L.; Touam, S.; Boumaza, A.; Boukhtouta, M.; Meradji, H.; Ghemid, S.; Omran, S. B.; Hassan, F. E. H.; Khenata, R. Phase stability and electronic behavior of MgS, MgSe and MgTe compounds. *Phase Transitions* **2017**, *90*, 929–941.
- (39) Kunduru, L.; Sripada, S.; Roshan, S. C. R.; Yedukondalu, N.; Sainath, M. Pressure induced semimetallic B2 phase of alkaline earth tellurides. *Journal of Physics: Conference Series* **2020**, *1495*, 012041.
- (40) Du, Y.; Tang, F.; Wang, D.; Sheng, L.; Kan, E.-j.; Duan, C.-G.; Savrasov, S. Y.; Wan, X. CaTe: a new topological node-line and Dirac semimetal. *npj Quantum Materials* **2017**, *2*, 3.
- (41) Kunduru, L.; Roshan, S. C. R.; Yedukondalu, N.; Sainath, M. Pressure driven topological semi metallic phase in SrTe. *AIP Conference Proceedings* **2018**, *1966*, 020029.

- (42) Varshney, D.; Jain, S.; Shriya, S.; Khenata, R. High-pressure and temperature-induced structural, elastic, and thermodynamical properties of strontium chalcogenides. *Journal of Theoretical and Applied Physics* **2016**, *10*, 163–193.
- (43) Musari, A. A.; Orukombo, S. A. Theoretical study of phonon dispersion, elastic, mechanical and thermodynamic properties of barium chalcogenides. *International Journal of Modern Physics B* **2018**, *32*, 1850092.
- (44) Muthaiah, R.; Garg, J. Thermal conductivity of magnesium selenide MgSe—A first principles study. *Computational Materials Science* **2021**, *198*, 110679.
- (45) Muthaiah, R.; Garg, J. Thermal conductivity of magnesium telluride MgTe - A first principles study. *Solid State Communications* **2021**, *337*, 114414.
- (46) Yang, Z.; Yuan, K.; Meng, J.; Zhang, X.; Tang, D.; Hu, M. Why thermal conductivity of CaO is lower than that of CaS: a study from the perspective of phonon splitting of optical mode. *Nanotechnology* **2020**, *32*, 025709.
- (47) Xia, Y.; Hodges, J. M.; Kanatzidis, M. G.; Chan, M. K. Y. Lattice thermal transport in group II-alloyed PbTe. *Applied Physics Letters* **2018**, *112*, 181906.
- (48) Seko, A.; Togo, A.; Hayashi, H.; Tsuda, K.; Chaput, L.; Tanaka, I. Prediction of Low-Thermal-Conductivity Compounds with First-Principles Anharmonic Lattice-Dynamics Calculations and Bayesian Optimization. *Phys. Rev. Lett.* **2015**, *115*, 205901.
- (49) Kresse, G.; Furthmüller, J. Efficient iterative schemes for ab initio total-energy calculations using a plane-wave basis set. *Phys. Rev. B* **1996**, *54*, 11169–11186.
- (50) Hellman, O.; Abrikosov, I. A.; Simak, S. I. Lattice dynamics of anharmonic solids from first principles. *Phys. Rev. B* **2011**, *84*, 180301.

- (51) Hellman, O.; Abrikosov, I. A. Temperature-dependent effective third-order interatomic force constants from first principles. *Phys. Rev. B* **2013**, *88*, 144301.
- (52) Hellman, O.; Steneteg, P.; Abrikosov, I. A.; Simak, S. I. Temperature dependent effective potential method for accurate free energy calculations of solids. *Phys. Rev. B* **2013**, *87*, 104111.
- (53) Hoover, W. G. Constant-pressure equations of motion. *Physical Review A* **1986**, *34*, 2499–2500.
- (54) Hoover, W. G. Canonical dynamics: Equilibrium phase-space distributions. *Physical Review A* **1985**, *31*, 1695–1697.
- (55) Luo, H.; Greene, R. G.; Ghandehari, K.; Li, T.; Ruoff, A. L. Structural phase transformations and the equations of state of calcium chalcogenides at high pressure. *Phys. Rev. B* **1994**, *50*, 16232–16237.
- (56) Zimmer, H. G.; Winzen, H.; Syassen, K. High-pressure phase transitions in CaTe and SrTe. *Phys. Rev. B* **1985**, *32*, 4066–4070.
- (57) Yamaoka, S.; Shimomura, O.; Nakazawa, H.; Fukunaga, O. Pressure-induced phase transformation in BaS. *Solid State Communications* **1980**, *33*, 87–89.
- (58) Syassen, K.; Christensen, N. E.; Winzen, H.; Fischer, K.; Evers, J. Optical response and band-structure calculations of alkaline-earth tellurides under pressure. *Phys. Rev. B* **1987**, *35*, 4052–4059.
- (59) Wyckoff, R. W. G. *Crystal Structures 1*, 2nd ed.; Crystal Structures; Interscience Publishers: New York, New York, 1963; Vol. 1.
- (60) Liu, L.-g.; Bassett, W. A. Effect of pressure on the crystal structure and the lattice parameters of BaO. *Journal of Geophysical Research (1896-1977)* **1972**, *77*, 4934–4937.

- (61) Yamaoka, S.; Shimomura, O.; Nakazawa, H.; Fukunaga, O. Pressure-induced phase transformation in BaS. *Solid State Communications* **1980**, *33*, 87–89.
- (62) Waag, A.; Heinke, H.; Scholl, S.; Becker, C.; Landwehr, G. Growth of MgTe and Cd_{1-x}Mg_xTe thin films by molecular beam epitaxy. *Journal of Crystal Growth* **1993**, *131*, 607–611.
- (63) Li, T.; Luo, H.; Greene, R. G.; Ruoff, A. L.; Trail, S. S.; Francis J. DiSalvo, J. High Pressure Phase of MgTe: Stable Structure at STP? *Physical Review Letters* **1995**, *74*, 5232–5235.
- (64) Duman, S.; Bağcı, S.; Tütüncü, H. M.; Srivastava, G. P. First-principles studies of ground-state and dynamical properties of MgS, MgSe, and MgTe in the rocksalt, zinc blende, wurtzite, and nickel arsenide phases. *Physical Review B* **2006**, *73*.
- (65) Chakrabarti, A. Role of NiAs phase in pressure-induced structural phase transitions in IIA-VI chalcogenides. *Physical Review B* **2000**, *62*, 1806–1814.
- (66) Camp, P. E. V.; Doren, V. E. V.; Martins, J. L. High-pressure phases of magnesium selenide and magnesium telluride. *Physical Review B* **1997**, *55*, 775–779.
- (67) Fei, Y. Effects of temperature and composition on the bulk modulus of (Mg,Fe)O. *American Mineralogist* **1999**, *84*, 272–276.
- (68) Richet, P.; Mao, H.-K.; Bell, P. M. Static compression and equation of state of CaO to 1.35 Mbar. *Journal of Geophysical Research: Solid Earth* **1988**, *93*, 15279–15288.
- (69) Pandey, R.; Sutjianto, A. Study of structural phase transition in MgSe. *Solid State Communications* **1994**, *91*, 269–271.
- (70) Bouad, N.; Chapon, L.; Marin-Ayral, R.-M.; Bouree-Vigneron, F.; Tedenac, J.-C. Neutron powder diffraction study of strain and crystallite size in mechanically alloyed PbTe. *Journal of Solid State Chemistry* **2003**, *173*, 189–195.

- (71) Baltache, H.; Khenata, R.; Sahnoun, M.; Driz, M.; Abbar, B.; Bouhafs, B. Full potential calculation of structural, electronic and elastic properties of alkaline earth oxides MgO, CaO and SrO. *Physica B: Condensed Matter* **2004**, *344*, 334–342.
- (72) Mir, S. H.; Jha, P. C.; Dabhi, S.; Jha, P. K. Ab initio study of phase stability, lattice dynamics and thermodynamic properties of magnesium chalcogenides. *Materials Chemistry and Physics* **2016**, *175*, 54–61.
- (73) Debnath, B.; Sarkar, U.; Debbarma, M.; Bhattacharjee, R.; Chattopadhyaya, S. Modification of band gaps and optoelectronic properties of binary calcium chalcogenides by means of doping of magnesium atom(s) in rock-salt phase- a first principle based theoretical initiative. *Journal of Solid State Chemistry* **2018**, *258*, 358–375.
- (74) Kürkcü, C. An Ab-initio Study of Structural and Electronic Properties of CaTe under High Pressure. *Russian Journal of Physical Chemistry A* **2019**, *93*, 2226–2232.
- (75) Drablia, S.; Boukhris, N.; Boulechfar, R.; Meradji, H.; Ghemid, S.; Ahmed, R.; Omran, S. B.; Hassan, F. E. H.; Khenata, R. Ab initio calculations of the structural, electronic, thermodynamic and thermal properties of BaSe_{1-x}Te_x alloys. **2017**, *92*, 105701.
- (76) Zhang, M.; Tang, G.; Li, Y. Hydrostatic Pressure Tuning of Thermal Conductivity for PbTe and PbSe Considering Pressure-Induced Phase Transitions. *ACS Omega* **2021**, *6*, 3980–3990.
- (77) Khenata, R.; Baltache, H.; Rérat, M.; Driz, M.; Sahnoun, M.; Bouhafs, B.; Abbar, B. First-principle study of structural, electronic and elastic properties of SrS, SrSe and SrTe under pressure. *Physica B: Condensed Matter* **2003**, *339*, 208–215.
- (78) Xue, F.; Wang, J.; Liu, X.; Sun, X. Study of electronic structure, elastic properties and thermodynamic properties of three PbTe phases: First-principles calculations. *Optik* **2021**, *232*, 166533.

- (79) Ren, Y. First principles study of electronic, phonon and elastic properties of rock-salt-phase MTe (M = Mg, Ca, Sr, Ba). *Computational Condensed Matter* **2017**, *11*, 69–76.
- (80) Son, P.; Bartels, R. CaO and SrO single crystal elastic constants and their pressure derivatives. *Journal of Physics and Chemistry of Solids* **1972**, *33*, 819–828.
- (81) Anderson, O. L.; Andreatch, P. Pressure Derivatives of Elastic Constants of Single-Crystal MgO at 23° and -195.8°C. *Journal of the American Ceramic Society* **1966**, *49*, 404–409.
- (82) Vetter, V.; Bartels, R. BaO single crystal elastic constants and their temperature dependence. *Journal of Physics and Chemistry of Solids* **1973**, *34*, 1448–1449.
- (83) Sinogeikin, S. V.; Bass, J. D. Single-crystal elasticity of MgO at high pressure. *Physical Review B* **1999**, *59*, R14141–R14144.
- (84) Cinthia, A. J.; Priyanga, G. S.; Rajeswarapalanichamy, R.; Iyakutti, K. Structural, electronic and mechanical properties of alkaline earth metal oxides MO (M=Be, Mg, Ca, Sr, Ba). *Journal of Physics and Chemistry of Solids* **2015**, *79*, 23–42.
- (85) Salam, M. M. A. First principles study of structural, elastic and electronic structural properties of strontium chalcogenides. *Chinese Journal of Physics* **2019**, *57*, 418–434.
- (86) Maizi, R.; Boudjahem, A.-G.; Boulbazine, M. First-Principles Investigations on Structural, Elastic, and Thermodynamic Properties of CaX (X = S, Se, and Te) under Pressure. *Russian Journal of Physical Chemistry A* **2019**, *93*, 2726–2734.
- (87) Wu, H.; Chen, Y.; Deng, C.; Han, X.; Yin, P. Electronic, elastic and dynamical properties of MgSe under pressure: rocksalt and iron silicide phase. *Philosophical Magazine* **2015**, *95*, 2240–2256.

- (88) Guo, Y.; Xia, D.; Liu, Q.; Zhao, X.; Li, J. Phase transition of CaTe induced by high-pressure: Structural and elastic DFT study of five structures. *Solid State Communications* **2021**, 114488.
- (89) Waller, I. *Dynamical Theory of Crystal Lattices* by M. Born and K. Huang. *Acta Crystallographica* **1956**, 9, 837–838.
- (90) Born, M. On the stability of crystal lattices. I. *Mathematical Proceedings of the Cambridge Philosophical Society* **1940**, 36, 160–172.
- (91) Haines, J.; Léger, J.; Bocquillon, G. Synthesis and Design of Superhard Materials. *Annual Review of Materials Research* **2001**, 31, 1–23.
- (92) Xiao, Y.; Chang, C.; Pei, Y.; Wu, D.; Peng, K.; Zhou, X.; Gong, S.; He, J.; Zhang, Y.; Zeng, Z. et al. Origin of low thermal conductivity in SnSe. *Phys. Rev. B* **2016**, 94, 125203.
- (93) Sanditov, D. S.; Belomestnykh, V. N. Relation between the parameters of the elasticity theory and averaged bulk modulus of solids. *Technical Physics* **2011**, 56, 1619–1623.
- (94) Jia, T.; Chen, G.; Zhang, Y. Lattice thermal conductivity evaluated using elastic properties. *Phys. Rev. B* **2017**, 95, 155206.
- (95) Fu, J.; Bernard, F.; Kamali-Bernard, S. First-principles calculations of typical anisotropic cubic and hexagonal structures and homogenized moduli estimation based on the Y-parameter: Application to CaO, MgO, CH and Calcite CaCO₃. *Journal of Physics and Chemistry of Solids* **2017**, 101, 74–89.
- (96) Khan, I.; Afaq, A.; Aliabad, H. R.; Ahmad, I. Transition from optically inactive to active Mg-chalcogenides: A first principle study. *Computational Materials Science* **2012**, 61, 278–282.

- (97) Bayrakci, M.; Colakoglu, K.; Deligoz, E.; Ciftci, Y. O. A first-principle study of the structural and lattice dynamical properties of CaX (X=S, Se, and Te). *High Pressure Research* **2009**, *29*, 187–203.
- (98) Syassen, K. Ionic monochalcogenides under pressure. *Physica B+C* **1986**, *139-140*, 277–283.
- (99) Saoud, F. S.; Rabah, K.; Bouhemadou, A.; Plenet, J. C.; Henini, M.; Djabou, R. E. H. Structural Stabilities and Elastic Thermodynamic Properties of SrTe Compound and SrTe_{1-x}Ca_x Alloy Under High Pressure. *Journal of Electronic Materials* **2016**, *46*, 766–774.
- (100) Lin, G. Q.; Gong, H.; Wu, P. Electronic properties of barium chalcogenides from first-principles calculations: Tailoring wide-band-gap II-VI semiconductors. *Physical Review B* **2005**, *71*.
- (101) Zagorac, D.; Doll, K.; Zagorac, J.; Jordanov, D.; Matović, B. Barium Sulfide under Pressure: Discovery of Metastable Polymorphs and Investigation of Electronic Properties on ab Initio Level. *Inorganic Chemistry* **2017**, *56*, 10644–10654.
- (102) Kholiya, K.; Verma, S. Pressure-induced phase transition and elastic properties of barium chalcogenides. *Phase Transitions* **2011**, *84*, 67–76.
- (103) Wang, J.; Yip, S.; Phillpot, S. R.; Wolf, D. Crystal instabilities at finite strain. *Phys. Rev. Lett.* **1993**, *71*, 4182–4185.
- (104) Yang, Y. L. Elastic moduli and band gap of PbTe under pressure: ab initio study. *Materials Science and Technology* **2012**, *28*, 1308–1313.
- (105) Madelung, O., Rössler, U., Schulz, M., Eds. *II-VI and I-VII Compounds; Semimagnetic Compounds*; Springer-Verlag, 1999.

- (106) Xia, Y.; Hegde, V. I.; Pal, K.; Hua, X.; Gaines, D.; Patel, S.; He, J.; Aykol, M.; Wolverton, C. High-Throughput Study of Lattice Thermal Conductivity in Binary Rocksalt and Zinc Blende Compounds Including Higher-Order Anharmonicity. *Physical Review X* **2020**, *10*.
- (107) Bagieva, G. Z.; Murtuzov, G. M.; Abdinova, G. D.; Allakhverdiev, E. A.; Abdinov, D. S. Influence of structural defects on the thermal conductivity of polycrystalline and single-crystal PbTe. *Inorganic Materials* **2012**, *48*, 789–791.
- (108) Xia, Y. Revisiting lattice thermal transport in PbTe: The crucial role of quartic anharmonicity. *Applied Physics Letters* **2018**, *113*, 073901.

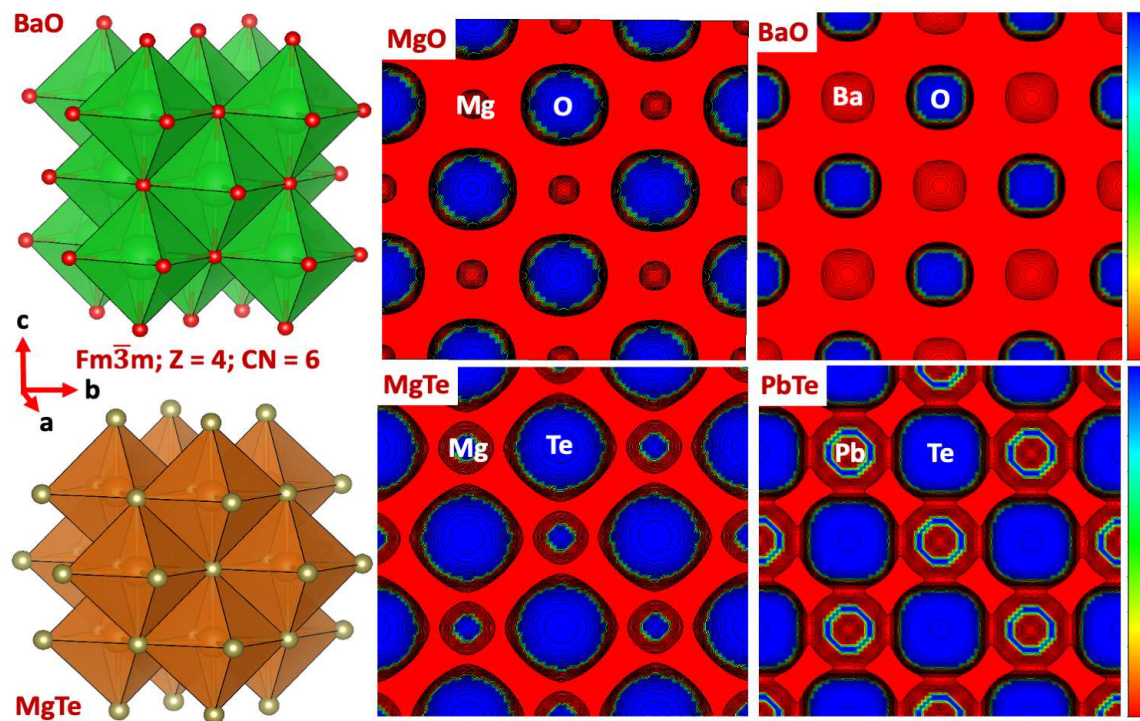


Figure 1: Crystal structure of BaO and MgTe, electron localization function (ELF) of MgO, BaO, MgTe and PbTe along (001) plane.

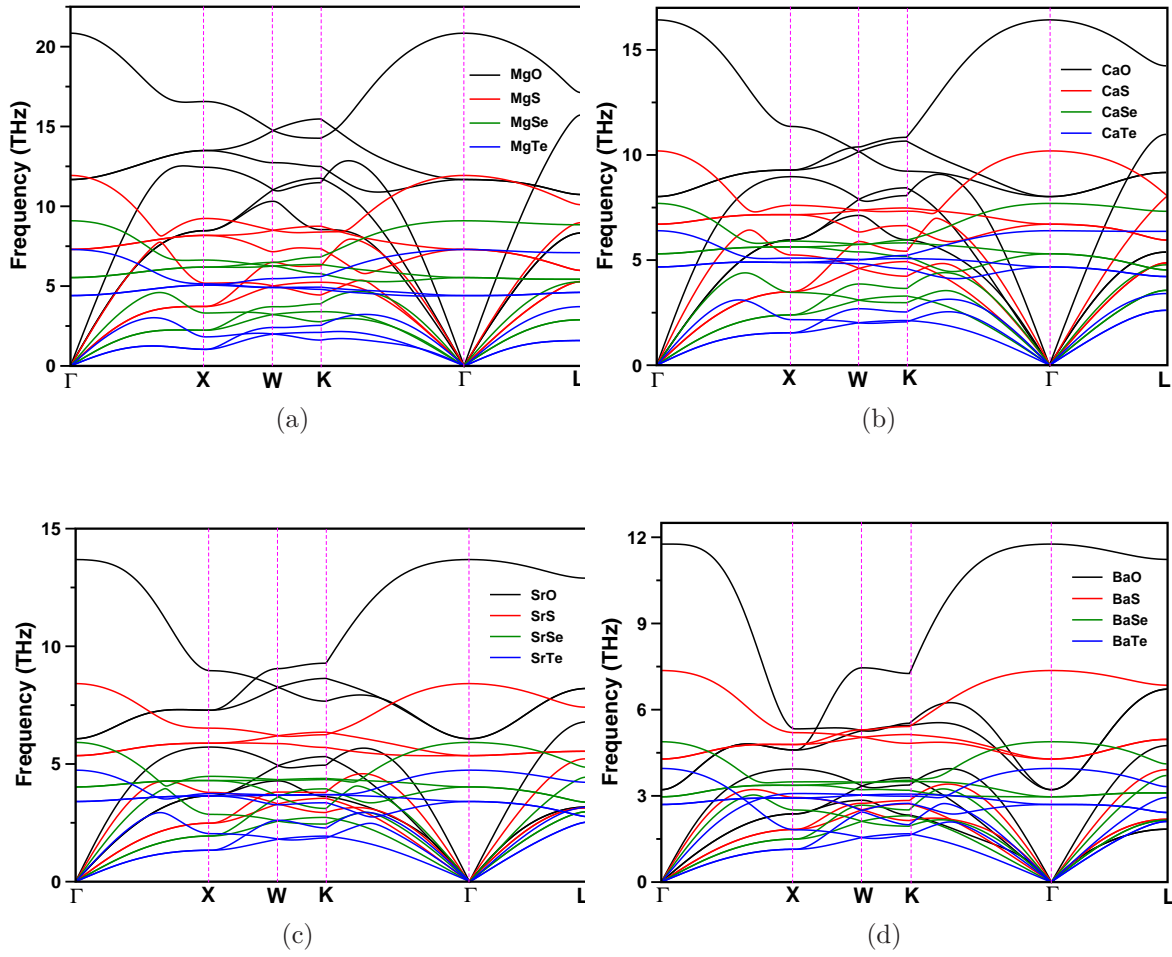


Figure 2: Calculated room temperature phonon dispersion curves of (a) MgX, (b) CaX, (c) SrX and (d) BaX compounds at PBEsol equilibrium volume; where X = O, S, Se and Te. Phonon softening is observed with increasing atomic mass of both alkaline-earth (Mg, Ca, Sr, Ba) and chalcogen (O, S, Se, Te) atoms.

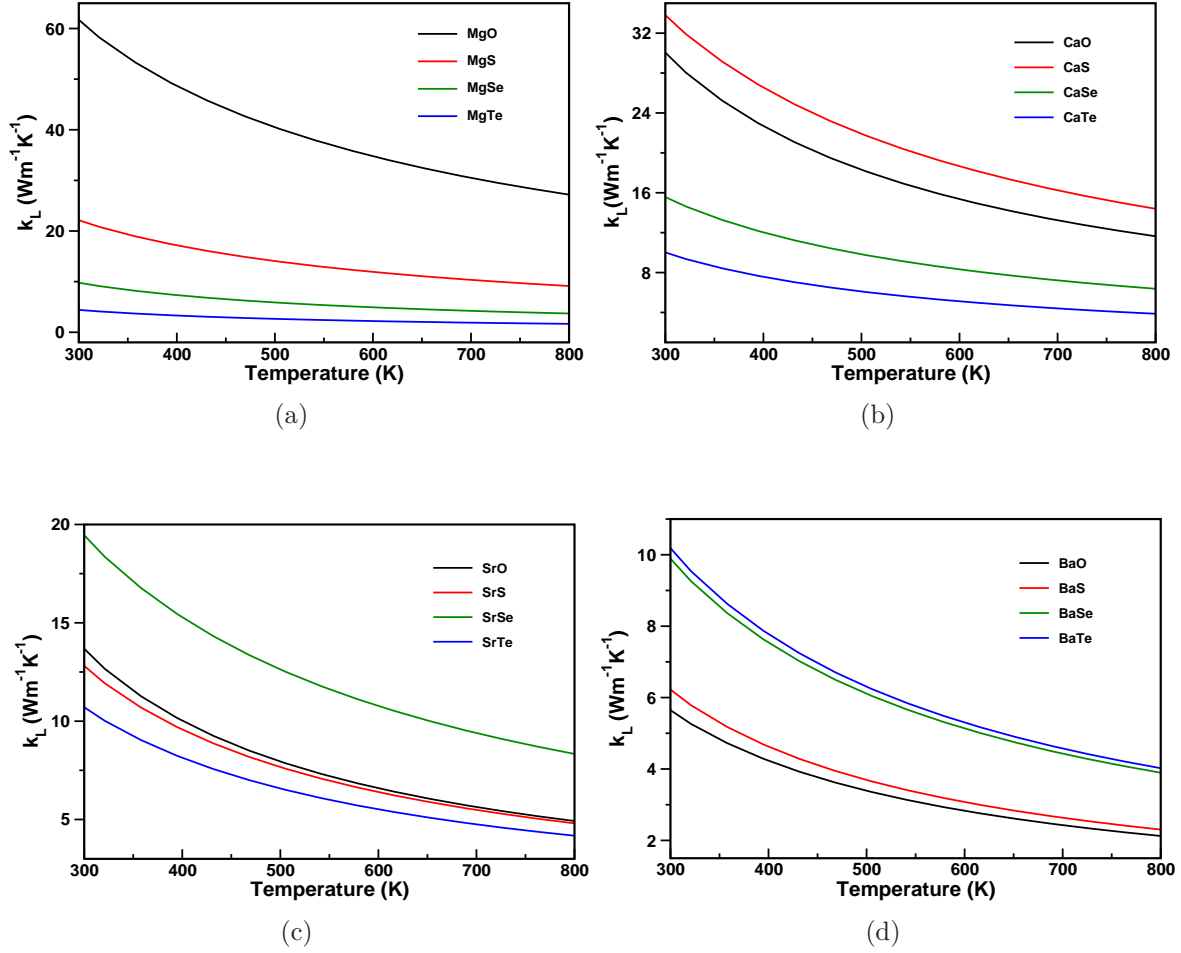


Figure 3: Calculated lattice thermal conductivity (k_L) of (a) MgX, (b) CaX, (c) SrX and (d) BaX compounds as a function of temperature; where X = O, S, Se and Te at PBEsol equilibrium volume. Anomalous trends are predicted for k_L partly in CaX (CaS > CaO > CaSe > CaTe), SrX (SrSe > SrO > SrS > SrTe) and completely opposite trend for BaX (BaTe > BaSe > BaS > BaO) compounds in contrast to the trends expected from their atomic mass.

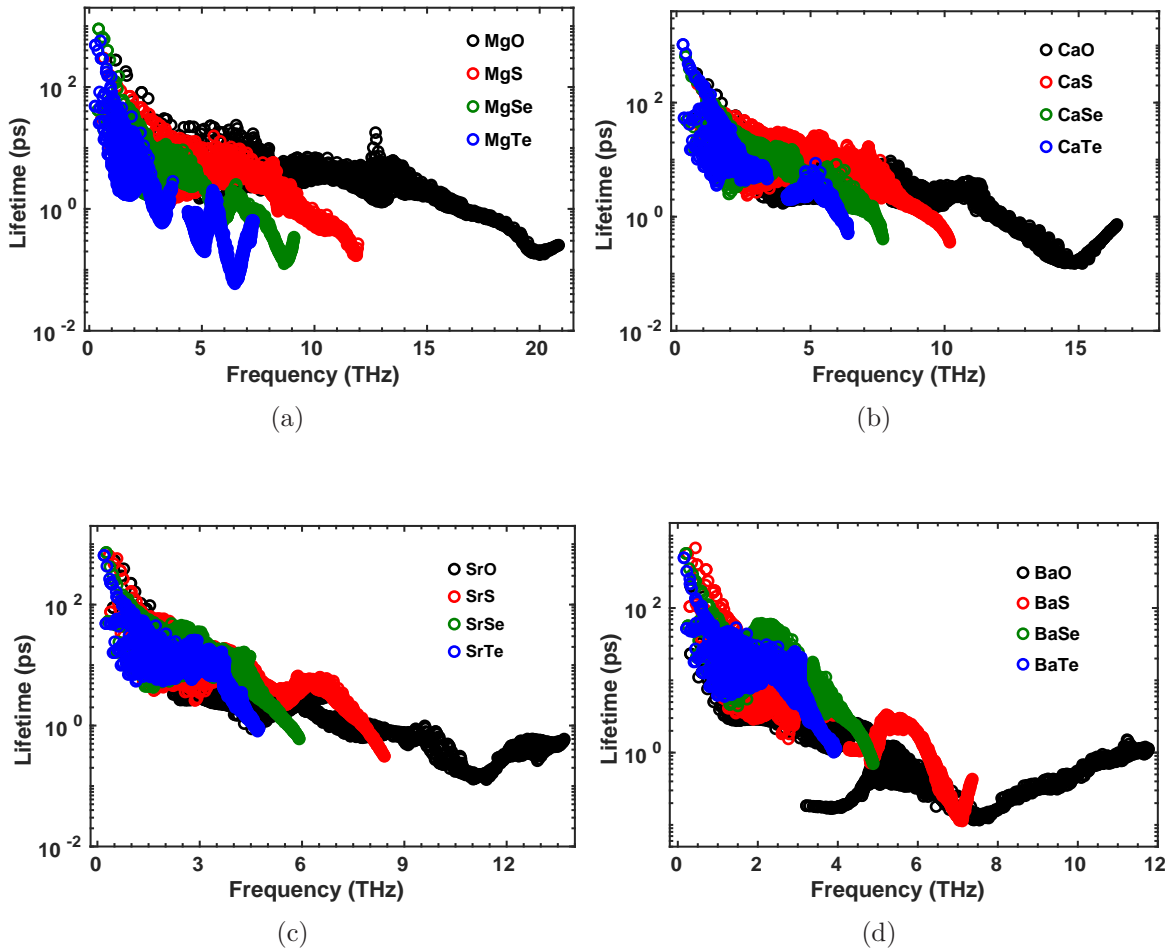


Figure 4: Calculated phonon lifetimes of (a) MgX, (b) CaX, (c) SrX and (d) BaX compounds as a function of frequency; where X = O, S, Se and Te.

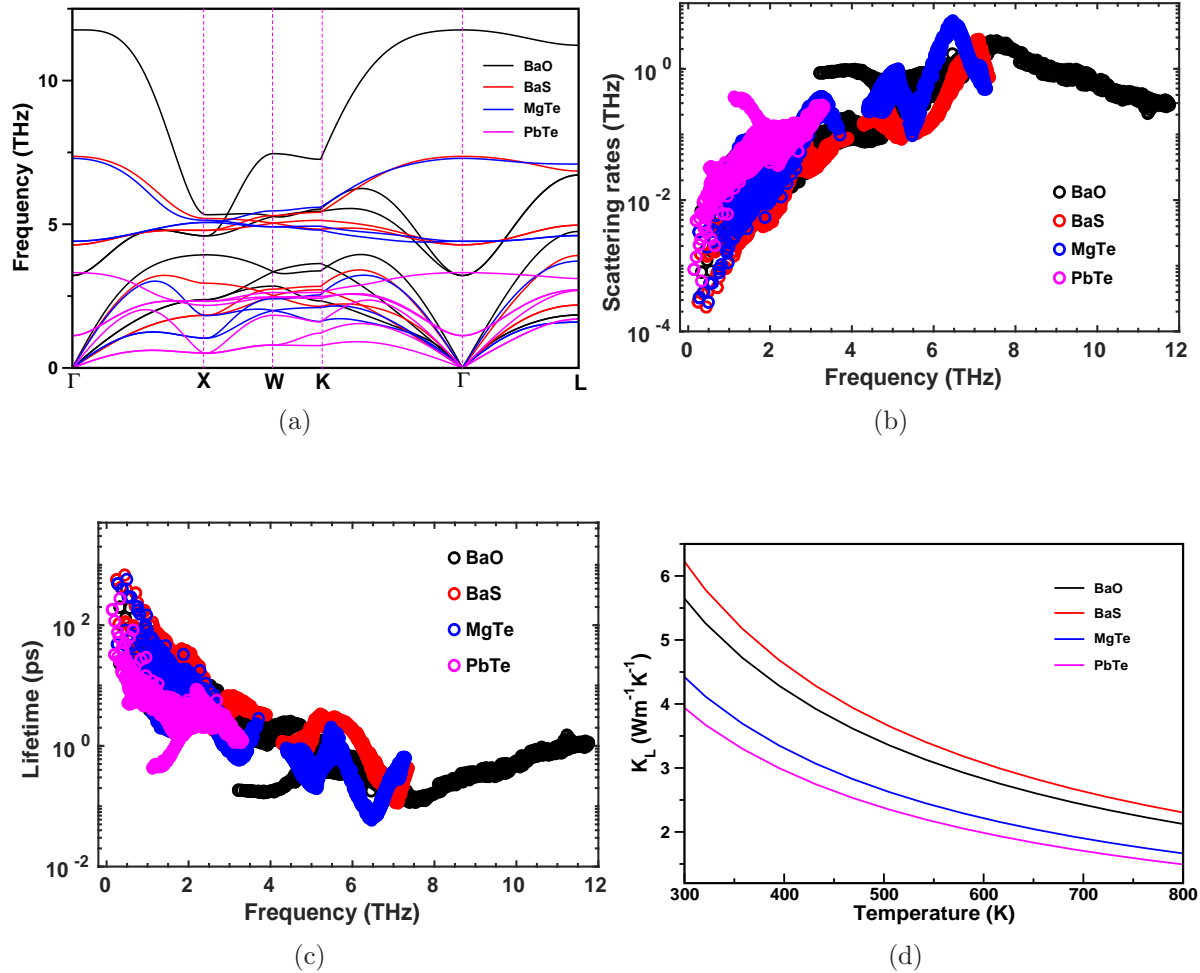


Figure 5: Calculated (a) phonon dispersion curves (b) phonon scattering rates (c) phonon lifetime, and (d) lattice thermal conductivity (k_L) of BaO, BaS, MgTe and PbTe compounds at PBEsol equilibrium volume. The obtained k_L values are decreasing in the following order: BaS > BaO > MgTe > PbTe.

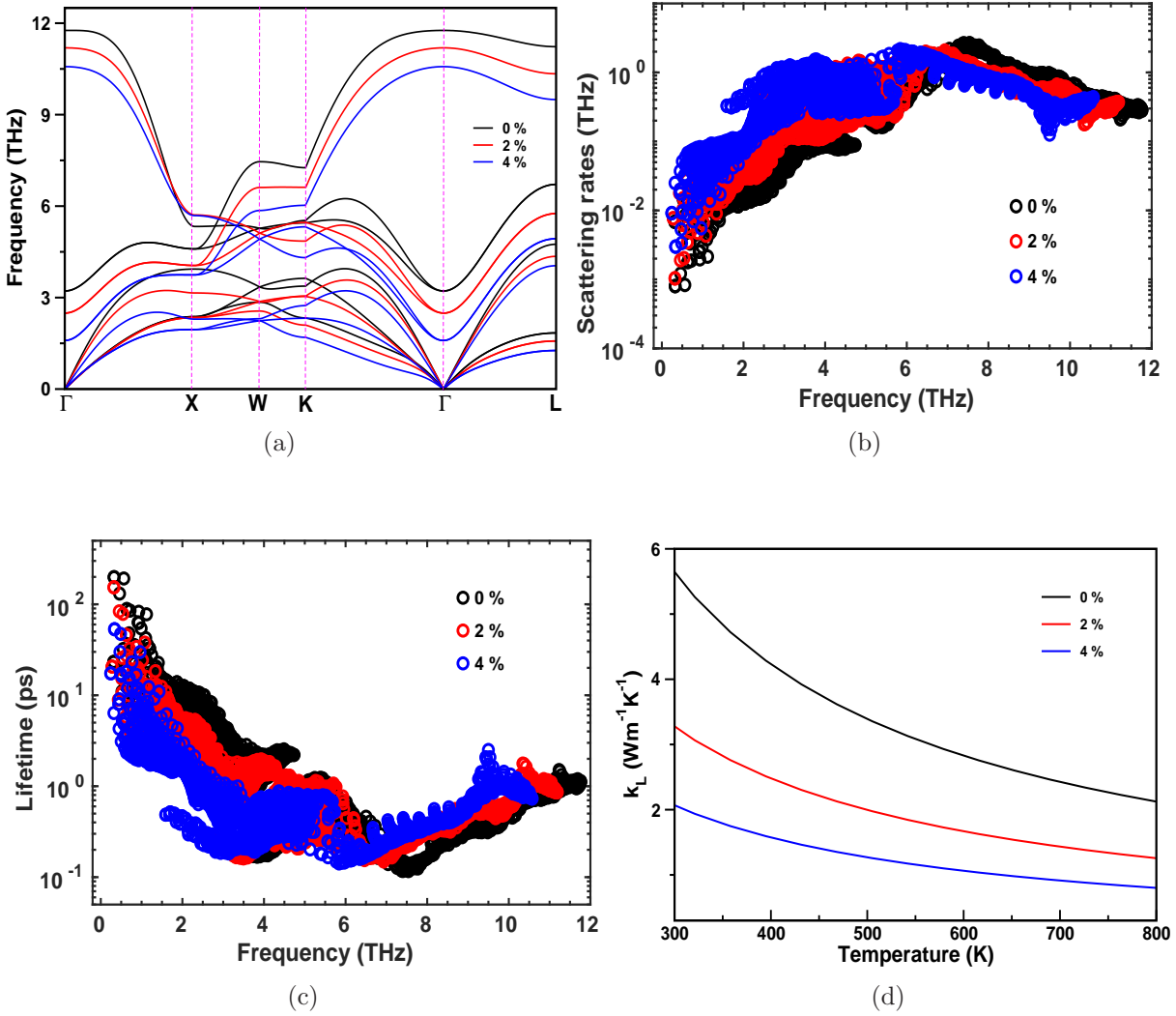


Figure 6: Calculated tensile strain dependent (a) phonon dispersion curves, (b) phonon scattering rates (c) phonon lifetime, and (d) lattice thermal conductivity (k_L) of BaO.

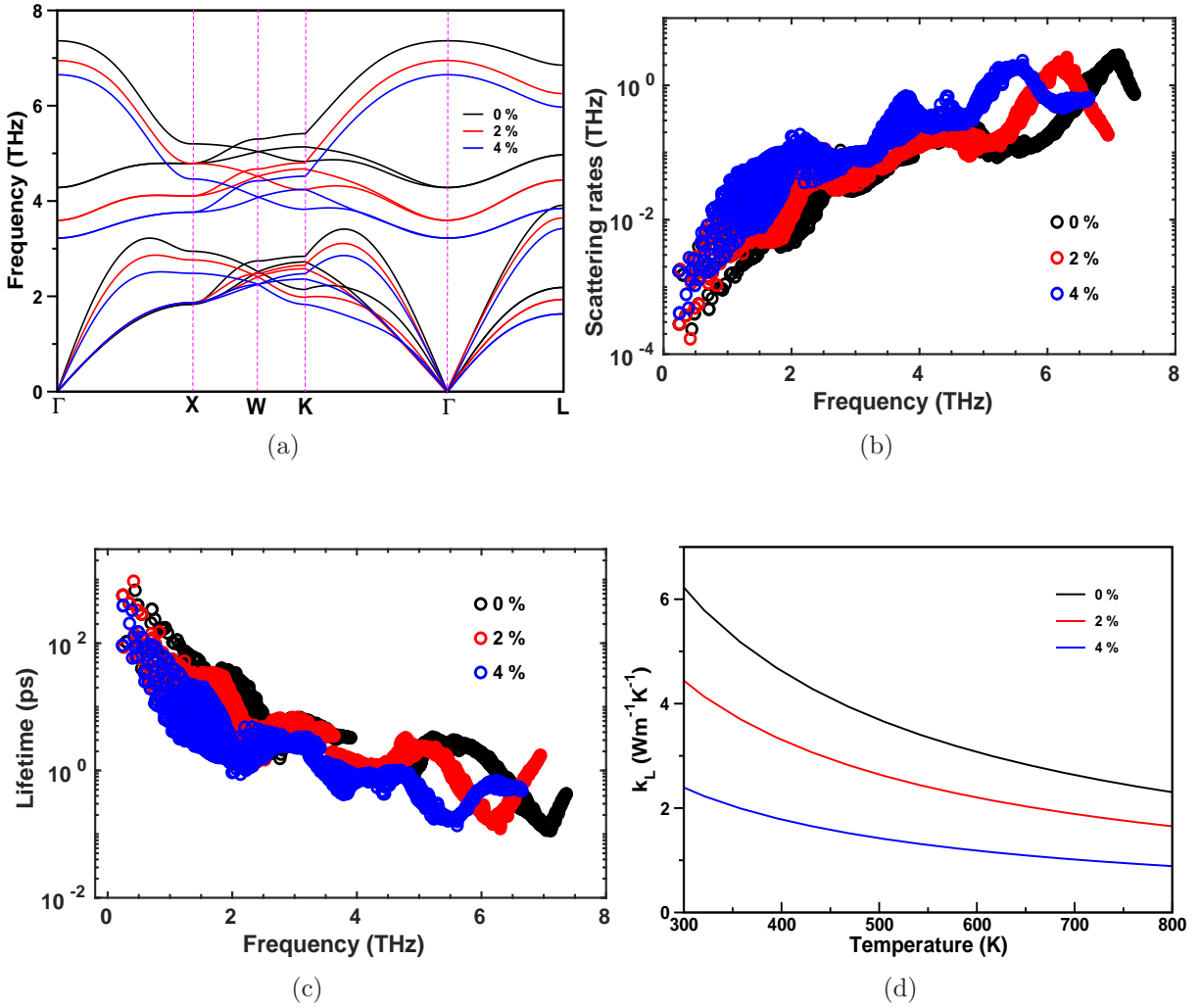


Figure 7: Calculated tensile strain dependent (a) phonon dispersion curves, (b) phonon scattering rates (c) phonon lifetime, and (d) lattice thermal conductivity (k_L) of BaS.

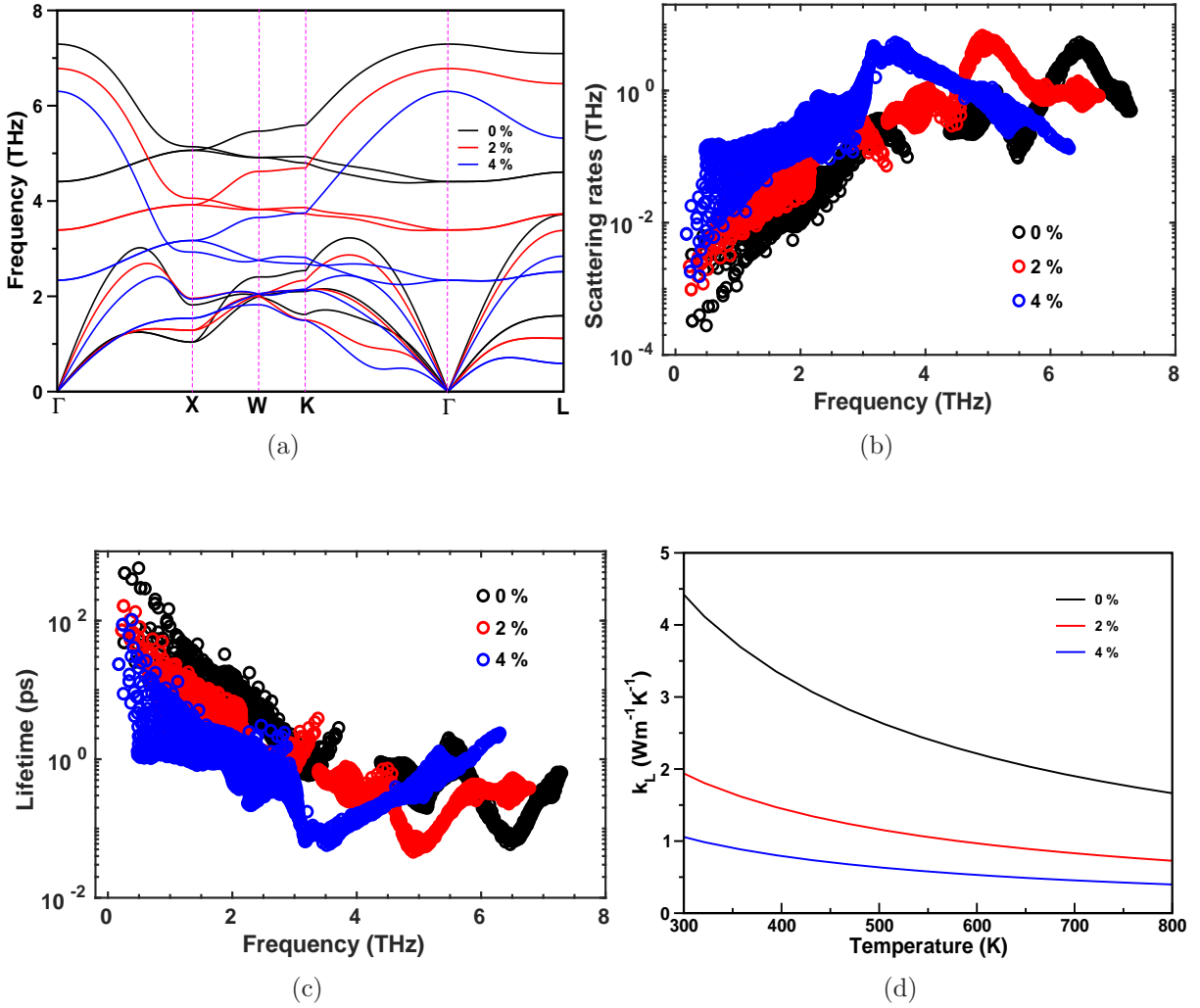
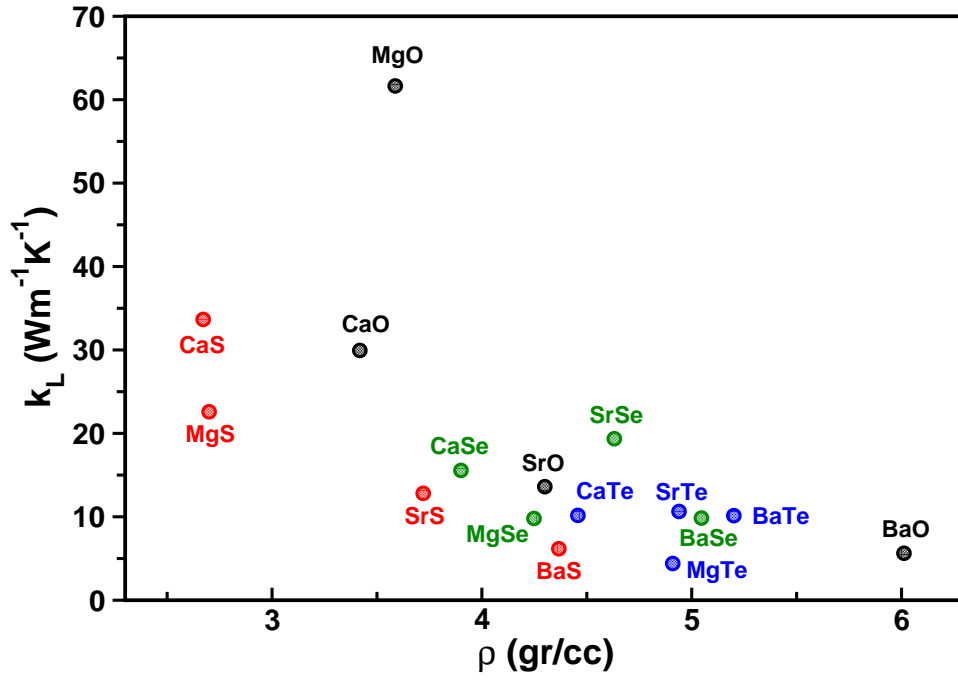
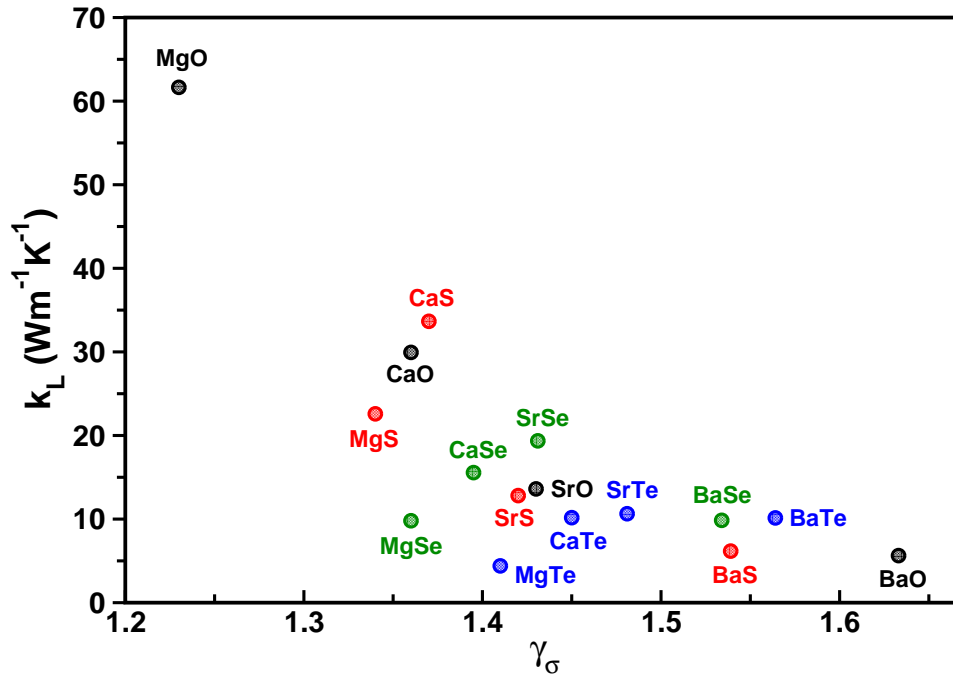


Figure 8: Calculated tensile strain dependent (a) phonon dispersion curves, (b) phonon scattering rates (c) phonon lifetime, and (d) lattice thermal conductivity (k_L) of MgTe.

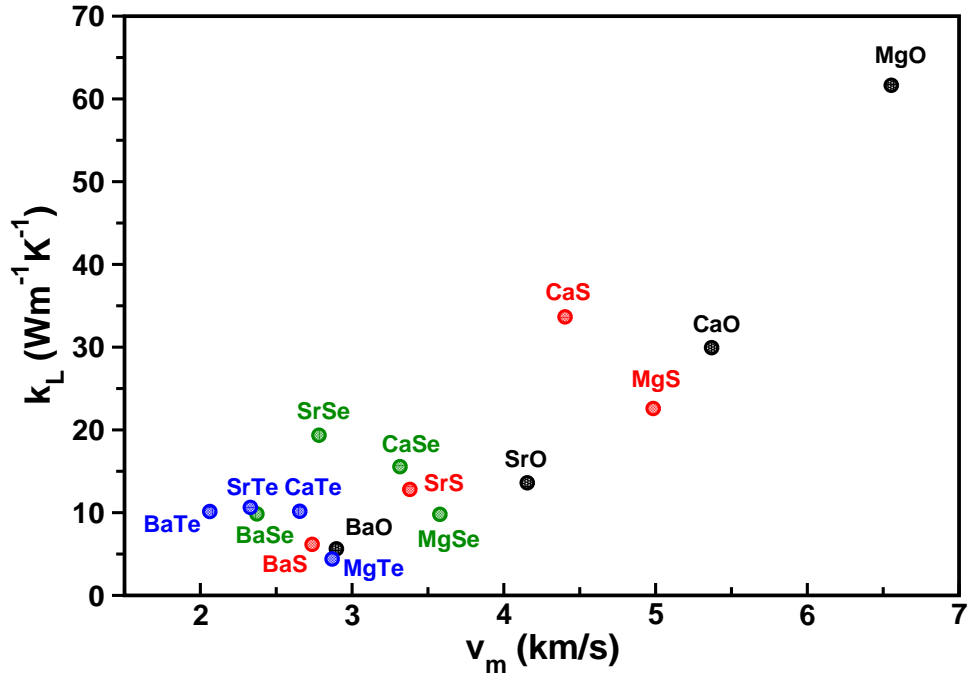


(a)

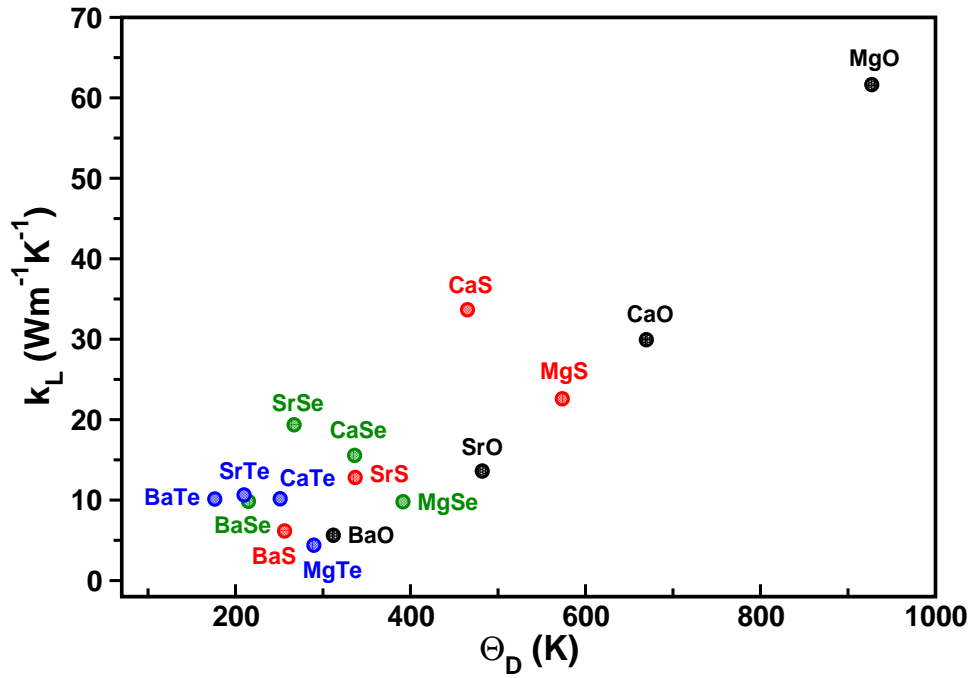


(b)

Figure 9: Calculated k_L as a function of (a) density (ρ) and (b) Grüneisen parameter (γ_σ) for 16 MX compounds.



(a)



(b)

Figure 10: Calculated k_L as a function of (a) average (v_m) sound velocity (b) Debye temperature (Θ_D) for 16 MX compounds.

Table 1: Calculated equilibrium lattice constant (a, in Å) of MX compounds at ambient pressure and are compared with available X-ray diffraction data and other first principles calculations.

Compound	This work	Expt.	Others
MgO	4.210	4.21 ^a	4.165 ^b , 4.2130 ^c
MgS	5.176	5.2033 ^d	5.19 ^e , 5.234 ^f , 5.2018 ^g
MgSe	5.445	5.463 ^h	5.46 ^e , 5.512 ^f , 5.4823 ^g
MgTe	5.901	-	5.98 ^e , 5.980 ^f , 5.9585 ^g
CaO	4.776	4.81 ⁱ	4.72 ^b , 4.828 ^j
CaS	5.639	5.689 ^k	5.67 ^l , 5.712 ^j , 5.637 ^m
CaSe	5.874	5.916 ^k	5.91 ^l , 5.965 ^j , 5.868 ^m
CaTe	6.298	6.348 ^k , 6.356 ⁿ	6.33 ^l , 6.399 ^j , 6.4430 ^o
SrO	5.134	5.16 ^p	5.073 ^b , 5.184 ^q
SrS	5.978	6.024 ^r	6.076 ^s , 6.05 ^q
SrSe	6.205	6.236 ^k	6.323 ^s , 6.3 ^q
SrTe	6.614	6.66 ^t , 6.659 ⁿ	6.76 ^s , 6.718 ^q , 6.66 ^u , 6.683 ^u
BaO	5.533	5.520 ^v	5.562 ^w , 5.454 ^w , 5.614 ^x
BaS	6.363	6.387 ^y	6.44 ^z , 6.38998 ^{aa} , 6.407 ^w , 6.455 ^x
BaSe	6.578	6.59 ^{ab}	6.59298 ^{aa} , 6.640 ^w , 6.699 ^x , 6.668 ^{ac}
BaTe	6.968	6.99 ^{ab}	7.00598 ^a , 6.989 ^w , 7.080 ^x , 7.075 ^{ac}
PbTe	6.441	6.46 ^{ad}	6.45 ^{ae} , 6.35 ^{af} , 6.576 ^{ag}

^aRef. ⁶⁷ ^bRef. ⁷¹ ^cRef. ⁹⁵ ^dRef. ⁵⁹ ^eRef. ⁹⁶ ^fRef. ³⁸ ^gRef. ⁷² ^hRef. ⁶⁹ ⁱRef. ⁶⁸ ^jRef. ¹⁷ ^kRef. ⁵⁵ ^lRef. ⁹⁷
^mRef. ⁷³ ⁿRef. ⁵⁶ ^oRef. ⁷⁴ ^pRef. ⁶⁰ ^qRef. ¹⁸ ^rRef. ⁵⁸ ^sRef. ⁷⁷ ^tRef. ⁹⁸ ^uRef. ⁹⁹ ^vRef. ⁶¹ ^wRef. ¹⁰⁰
^xRef. ¹⁹ ^yRef. ⁵⁷ ^zRef. ¹⁰¹ ^{aa}Ref. ¹⁰² ^{ab}Ref. ¹⁰³ ^{ac}Ref. ⁷⁵ ^{ad}Ref. ⁷⁰ ^{ae}Ref. ⁷⁶ ^{af}Ref. ¹⁰⁴ ^{ag}Ref. ⁷⁸

Table 2: Calculated lattice thermal conductivity (k_L , in $\text{Wm}^{-1}\text{K}^{-1}$) at 300 K for 16 MX and PbTe compounds.

Compound	This work		Expt.	Others			Others
	k_L	k_L^E		k_{3ph}^{HA}	k_{3ph}^{SCPH}	$k_{3,4ph}^{SCPH}$	
MgO	61.65	61.65	52 ^a	52.1 ^b	58.7 ^b	50.1 ^b	-
MgS	22.59	18.74	-	-	-	-	-
MgSe	9.8	7.55	-	-	-	-	-
MgTe	4.45	4.45	-	-	-	-	3.5 ^c , 3 ^d
CaO	29.94	24.77	30 ^a	21.3 ^b	25.1 ^b	22.2 ^b	-
CaS	33.66	28.39	-	-	-	-	-
CaSe	15.56	13.21	-	-	-	-	-
CaTe	10.17	8.33	-	-	-	-	3.1 ^c , 8.5 ^d
SrO	13.61	11.65	10 ^a	9.0 ^b	11.0 ^b	9.9 ^b	-
SrS	12.81	11.60	-	-	-	-	-
SrSe	19.36	15.8	-	-	-	-	-
SrTe	10.64	9.66	-	-	-	-	2.5 ^c , 10.5 ^d
BaO	5.63	6.76	3 ^a	2.8 ^b	4.4 ^b	3.3 ^b	-
BaS	6.17	6.28	-	-	-	-	-
BaSe	9.85	10.06	-	-	-	-	-
BaTe	10.14	9.84	-	-	-	-	1.9 ^c , 10.2 ^d
PbTe	3.93	3.21	3.1 ^e , 3.0 ^e	-	3.3 ^d	2.6 ^f	-
	-	-	2.38 ^e , 2.6 ^e	-	-	-	-

^aRef. ¹⁰⁵ ^bRef. ¹⁰⁶ ^c Ref. ⁷⁹ ^dRef. ⁴⁷ ^eRef. ¹⁰⁷ ^fRef. ¹⁰⁸

k_L : calculated at the PBEsol equilibrium lattice constant

k_L^E : calculated at the experimental lattice constant

Supporting Information

Anomalous Lattice Thermal Conductivity in Rocksalt IIA-VIA Compounds

S. C. Rakesh Roshan,^{*,†,‡} N. Yedukondalu,^{*,¶} Rajmohan Muthaiah,[§] K. Lavanya,^{||,⊥} P. Anees,[#] R. Rakesh Kumar,[@] T. Venkatappa Rao,[@] Lars Ehm,[¶]
and John B. Parise[¶]

[†]*Rajiv Gandhi University of Knowledge Technologies, Basar, Telangana-504107, India*

[‡]*Department of Physics, National Institute of Technology-Warangal, Telangana, India*

[¶]*Department of Geosciences, Center for Materials by Design, and Institute for Advanced Computational Science, State University of New York, Stony Brook, New York 11794-2100, USA*

[§]*School of Aerospace and Mechanical Engineering, University of Oklahoma, Norman, OK 73019, USA*

^{||}*Jawaharlal Nehru Technological University (JNTU), Hyderabad, 500085, Telangana, India.*

[⊥]*Telangana Social Welfare Residential Degree College for Women (TSWRDC-W), Nizamabad, 503002, Telangana, India.*

[#]*Materials Physics Division, Indira Gandhi Centre for Atomic Research, Kalpakkam 603102, Tamil Nadu, India*

[@]*Department of Physics, Nanomaterials and Energy Harvesting Research Lab, National Institute of Technology-Warangal, Telangana, India*

E-mail: roshan@rgukt.ac.in; nykondalu@gmail.com

Lattice thermal conductivity of MX compounds

We have also calculated lattice thermal conductivity (k_L) for MX compounds at the experimental lattice constant (see Table 2) by varying metal cation with fixed chalcogen atoms (see Figure S1) and vice versa (see Figure S2). As shown in Figure S1, the k_L values are decreasing with increasing atomic mass *i.e.*, from MgO > CaO > SrO > BaO in MO compounds. While anomalous trends are observed between MgS and CaS with the following trend for MS (CaS > MgS > SrS > BaS) compounds, for MSe (SrSe > CaSe > BaSe > MgSe) and MTe (BaTe > SrTe > CaTe > MgTe) compounds. Especially, MTe series shows an opposite trend for k_L in contrary to the expected trend from their atomic mass.

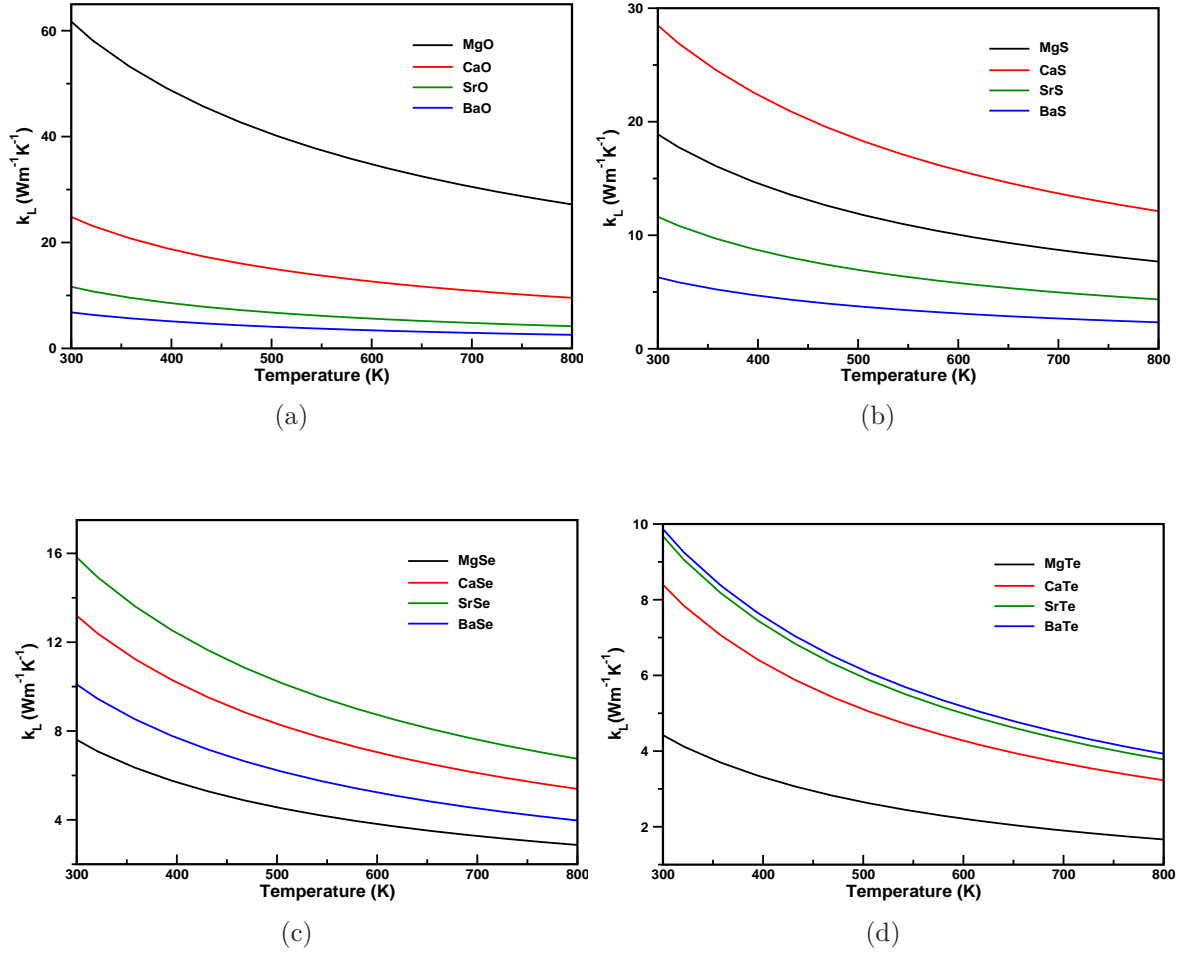


Figure S1: Calculated lattice thermal conductivity of (a) MO, (b) MS, (c) MSe and (d) MTe compounds as a function of temperature at the experimental lattice constant; where M = Mg, Ca, Sr and Ba.

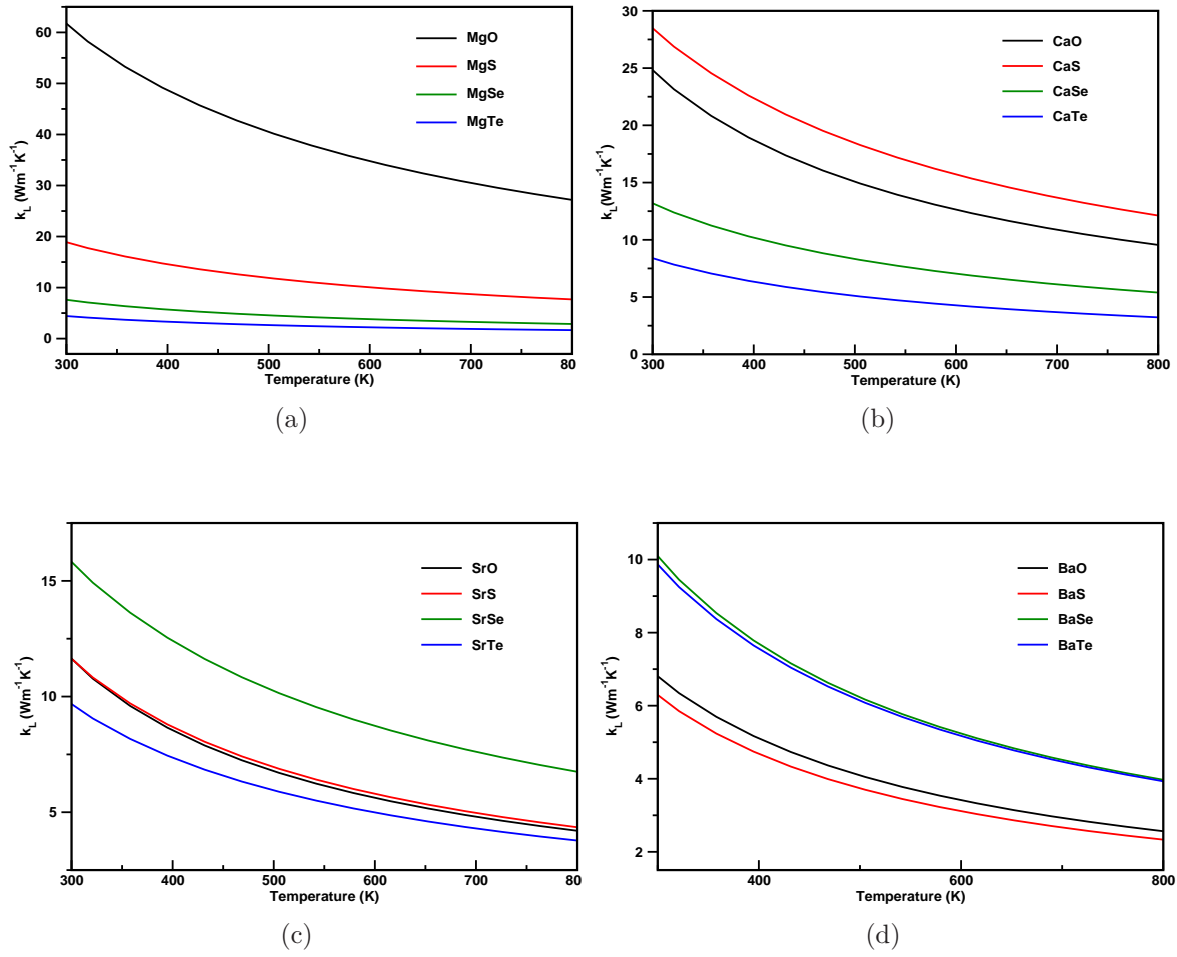


Figure S2: Calculated lattice thermal conductivity of (a) MgX, (b) CaX, (c) SrX and (d) BaX compounds as a function of temperature at the experimental lattice constant; where X = O, S, Se and Te.

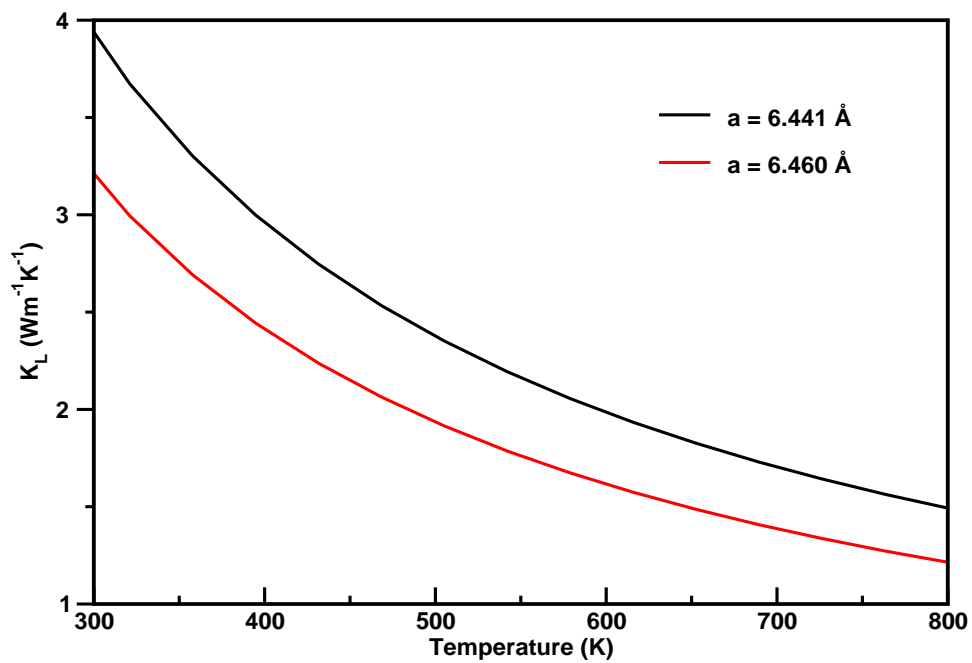


Figure S3: Calculated lattice thermal conductivity of PbTe at equilibrium lattice constant ($a = 6.441 \text{ \AA}$) using PBEsol and experimental lattice constant ($a = 6.460 \text{ \AA}$). This clearly shows sensitivity of k_L against lattice constant for PbTe.

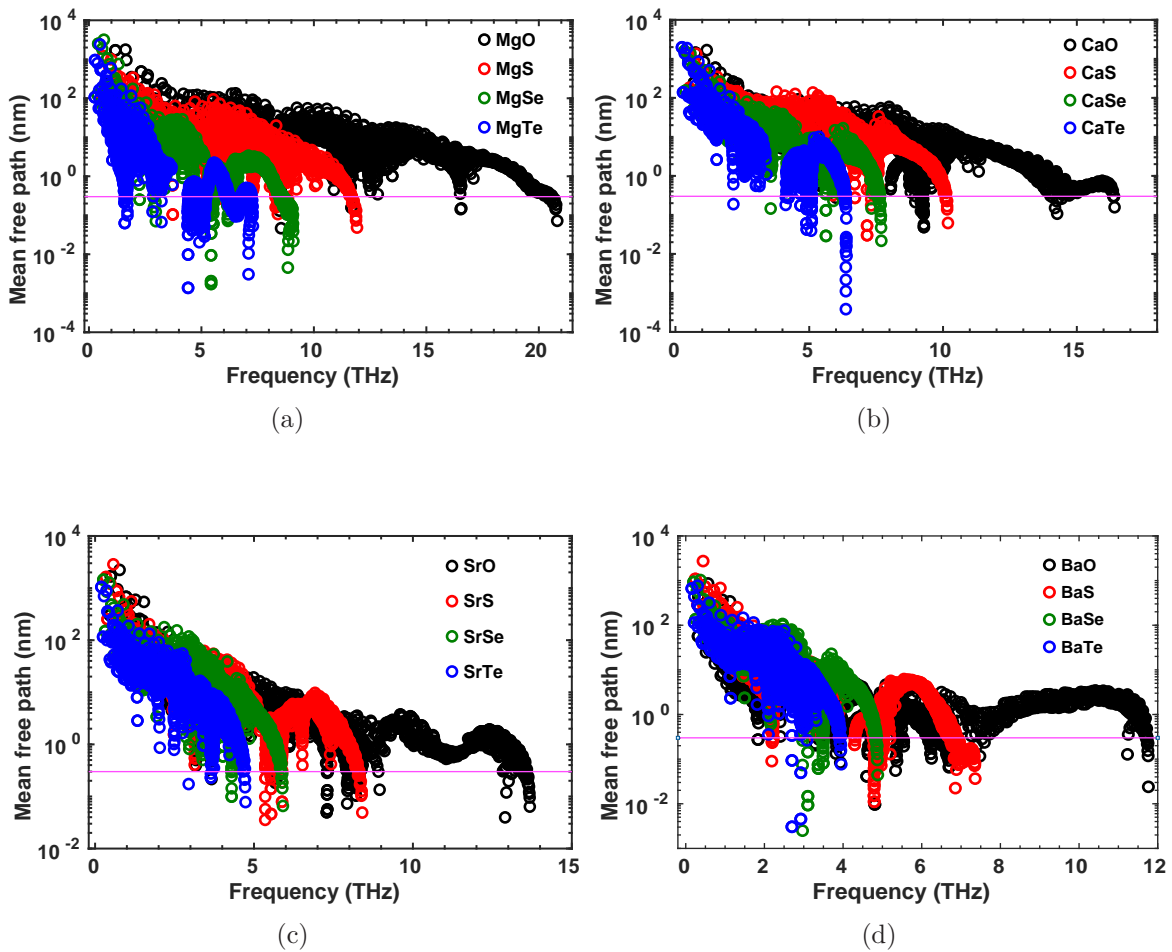


Figure S4: Calculated mean free paths of (a) MgX, (b) CaX, (c) SrX and (d) BaX compounds as a function of frequency; where X = O, S, Se and Te. The horizontal solid line (magenta) represents Ioffe-Regel limit for mean free paths.

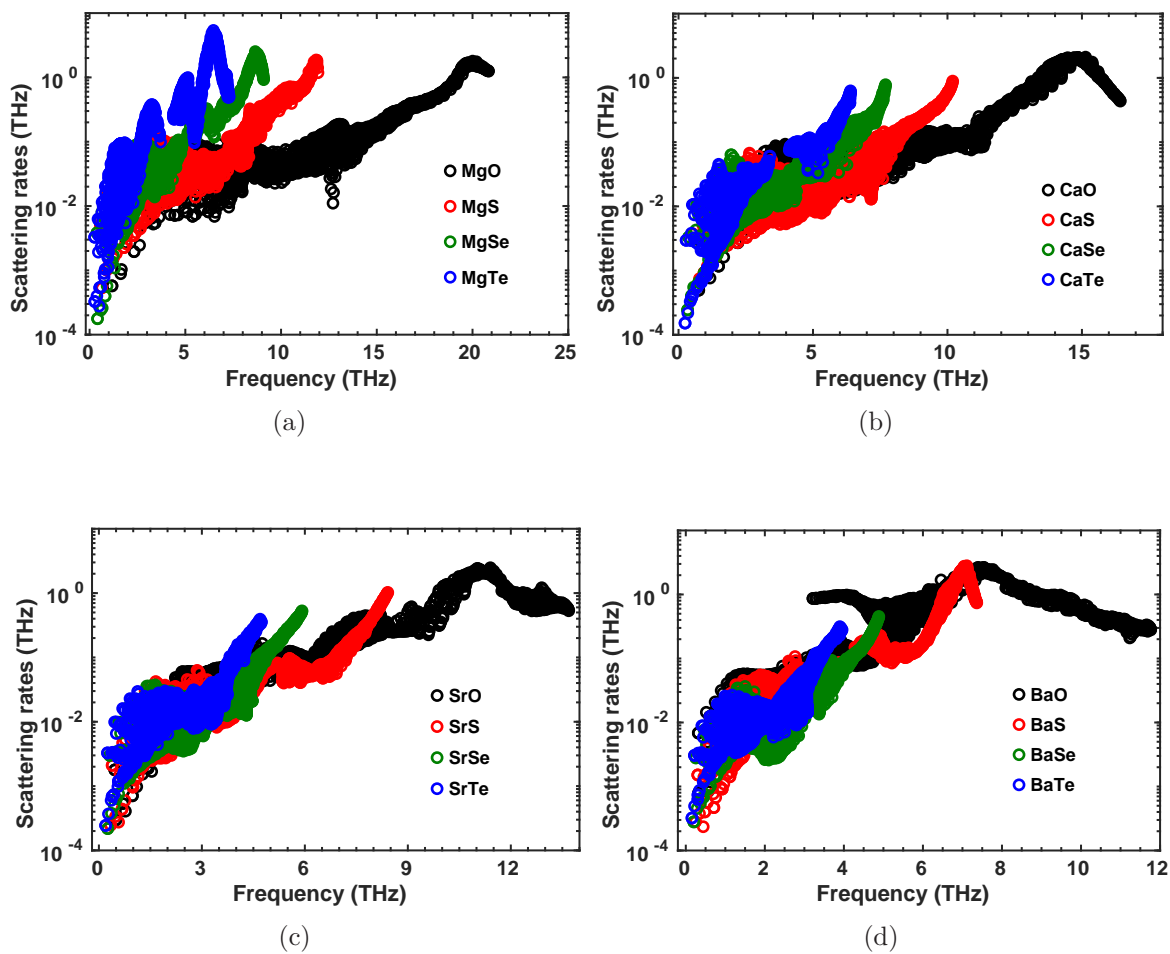


Figure S5: Calculated scattering rates of (a) MgX, (b) CaX, (c) SrX and (d) BaX compounds as a function of frequency; where X = O, S, Se and Te.

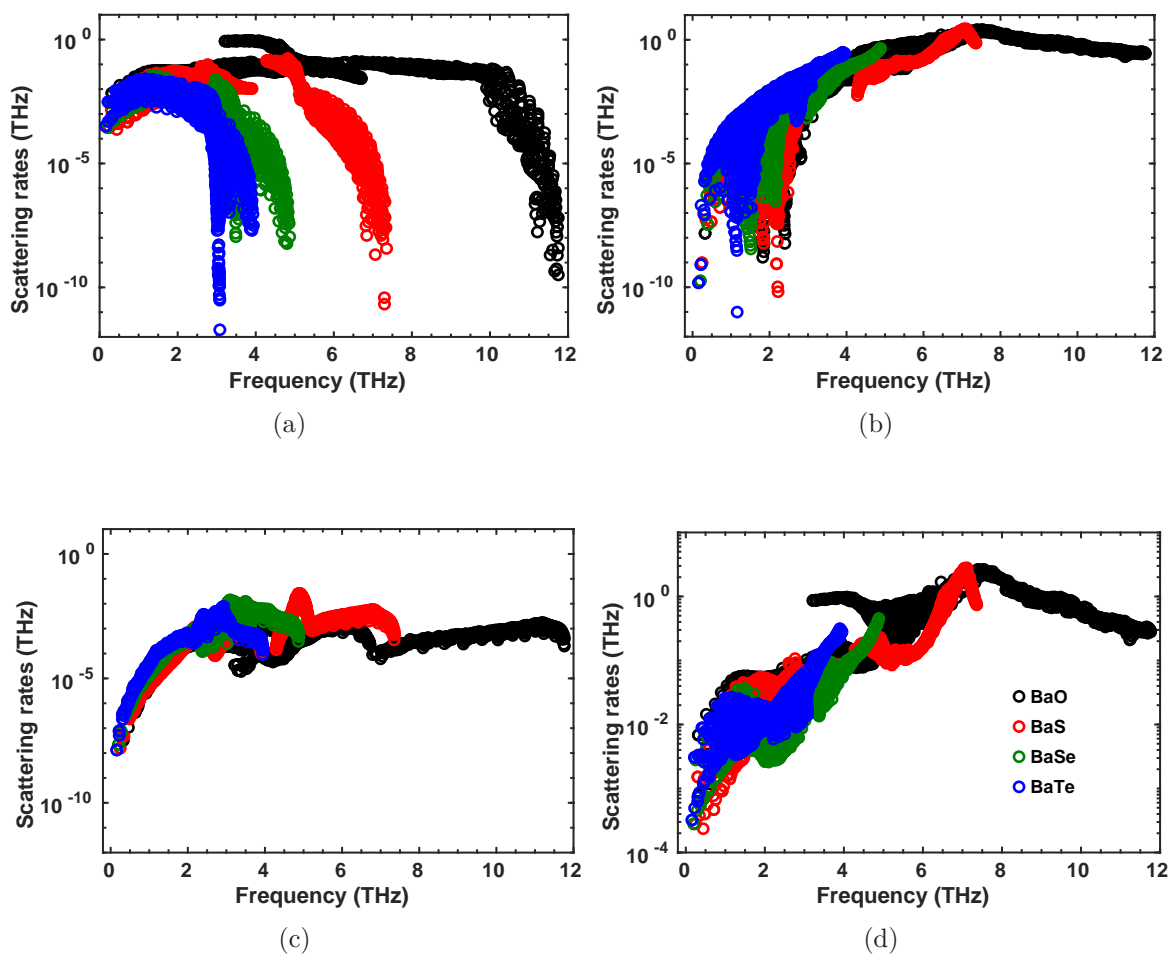
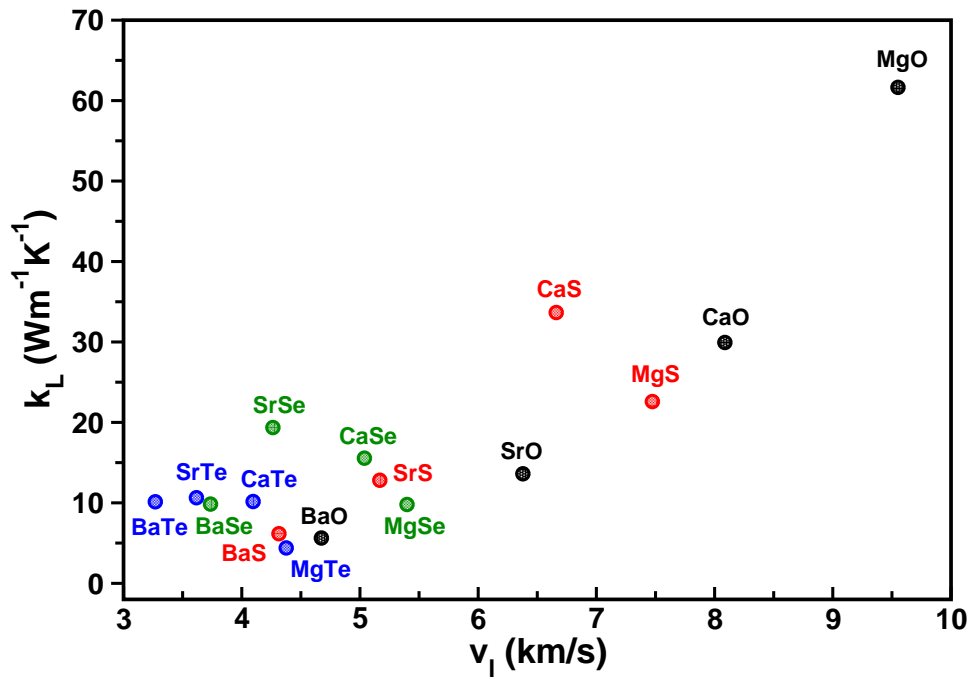
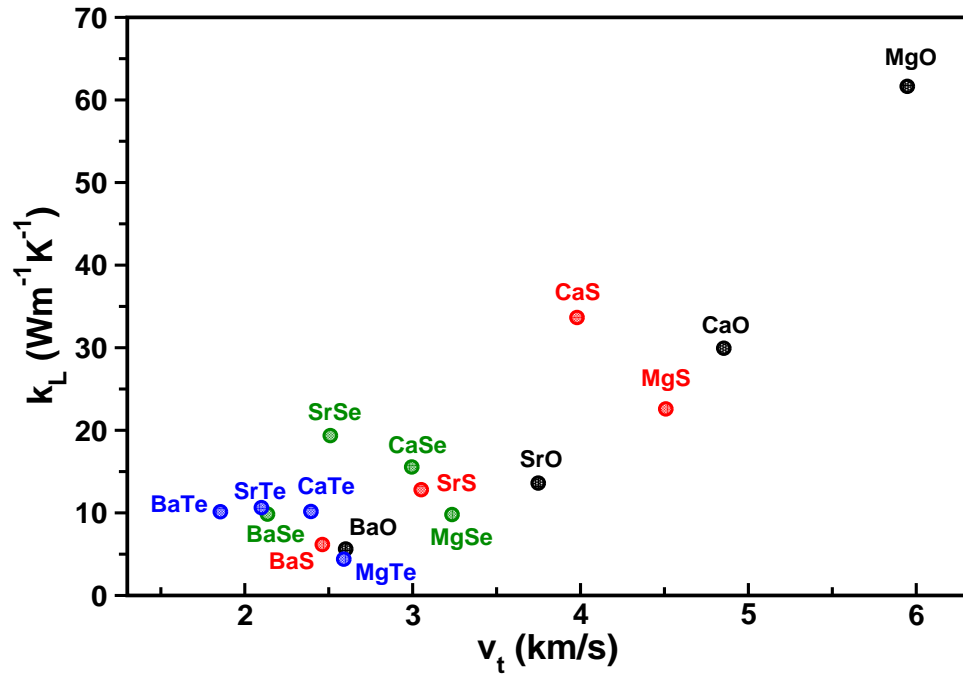


Figure S6: Calculated (a) absorption (b) emission (c) isotope and (d) total scattering rates of BaX (X = O, S, Se and Te) compounds as a function of frequency.



(a)



(b)

Figure S7: Calculated k_L as a function of (a) longitudinal (v_l) (b) transverse (v_t) sound velocities for 16 MX compounds.

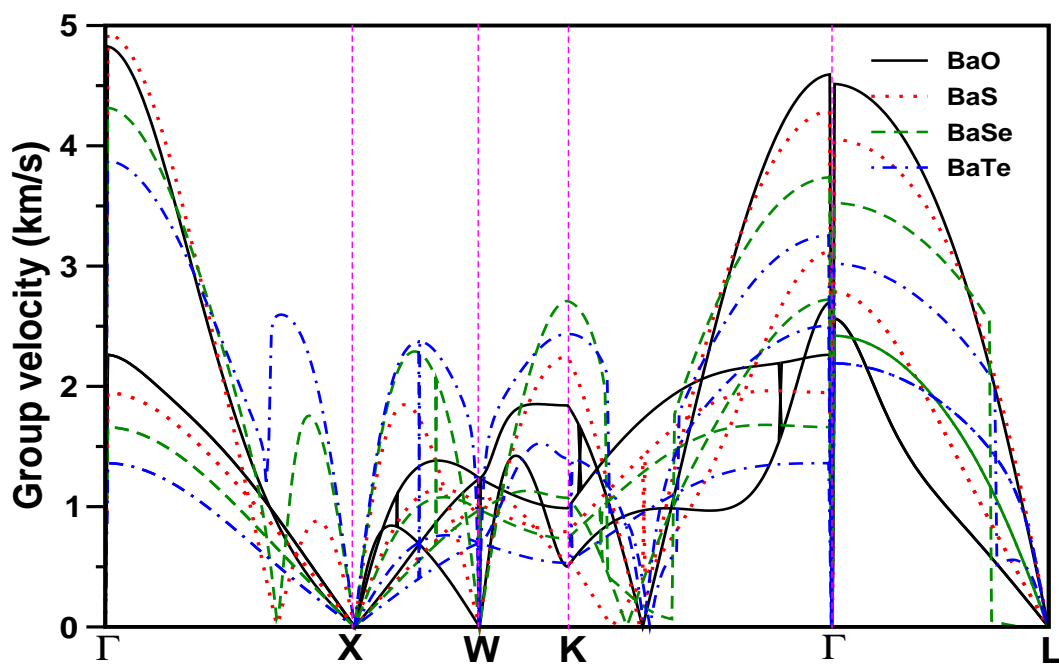


Figure S8: Calculated phonon group velocities of BaX (X = O, S, Se and Te) compounds along high symmetry directions of the Brillouin zone.

Table S1: Calculated transverse optical (ω_{TO} , in cm^{-1}), longitudinal optical (ω_{LO} , in cm^{-1}) phonon modes and difference between LO and TO modes ($\omega_{LO}-\omega_{TO}$, in cm^{-1}) at 300 K for 16 MX compounds are compared with the available experimental and previous first principles calculations. The values given in parenthesis are in THz units.

Compound	Method	ω_{TO}	ω_{LO}	$\omega_{LO}-\omega_{TO}$
MgO	This work	390.11 (11.68)	696.06 (20.84)	305.94 (9.16)
MgS	This work	243.82 (7.3)	398.46 (11.93)	154.64 (4.63)
	others	220.64 ^a , 224.9 ^b	385.06 ^a , 381.9 ^b	165.06
MgSe	This work	185.04 (5.54)	331.33 (9.92)	146.29 (4.38)
	others	171 ^c , 169.92 ^a	296 ^c , 292.31 ^a	123.31
MgTe	This work	147.29 (4.41)	243.49 (7.29)	96.19 (2.88)
	others	136.38 ^a , 141 ^d	236.06 ^a , 234.1 ^d	99.68
CaO	This work	317.63 (9.51)	588.51 (17.62)	270.87 (8.11)
	Expt	311 ^e	585 ^e	-
CaS	This work	224.11 (6.71)	340.35 (10.19)	116.23 (3.48)
	others	231.42 ^b	336.65 ^b	-
	Expt	229 ^f	342 ^f	-
CaSe	This work	177.02 (5.3)	257.18 (7.7)	80.16 (2.4)
	others	178.4 ^d	251.4 ^d	-
	Expt	168 ^f	220 ^f	-
CaTe	This work	155.98 (4.67)	213.76 (6.4)	57.78 (1.73)
	others	156.2 ^d	209 ^d	-

^aRef. ¹ ^b Ref. ² ^c Ref. ³ ^d Ref. ⁴ ^e Ref. ⁵ ^f Ref. ⁶ ^g Ref. ⁷ ^h Ref. ⁸ ⁱ Ref. ⁹

Table S1 continued

Compound	Method	ω_{TO}	ω_{LO}	$\omega_{LO}-\omega_{TO}$
SrO	This work	202.74 (6.07)	457.25 (13.69)	254.51 (7.62)
	others	217.85 ^g	474.13 ^g	-
	Expt	224.15 ^h	484.99 ^h	-
SrS	This work	179.02 (5.36)	280.90 (8.41)	101.87 (3.05)
	others	194.045 ⁱ	290.577 ⁱ	-
SrSe	This work	136.60 (4.03)	197.73 (5.92)	63.13 (1.89)
	others	127.496 ⁱ	193.193 ⁱ	-
SrTe	This work	113.90 (3.41)	158.32 (4.74)	44.42 (1.33)
	others	110.717 ⁱ	156.738 ⁱ	-
BaO	This work	107.55 (3.22)	392.78 (11.76)	285.24 (8.54)
	Expt	146 ^e	440 ^e	-
BaS	This work	142.95 (4.28)	245.82 (7.36)	102.87 (3.08)
	Expt	150 ^f	246 ^f	-
BaSe	This work	99.19 (2.97)	162.99 (4.88)	63.79 (1.91)
	Expt	100 ^f	156 ^f	-
BaTe	This work	90.18 (2.7)	131.93 (3.95)	41.75 (1.25)

^e Ref. ⁵ ^f Ref. ⁶

Table S2: Calculated second order elastic constants (C_{11} , C_{12} , C_{44} , in GPa) for MX compounds in rocksalt structure type.

Compound	This work			Others		
	C_{11}	C_{12}	C_{44}	C_{11}	C_{12}	C_{44}
MgO	298.03	88.15	143.96	297 ^a	99.6 ^a	151.9 ^a
	296.47 ^b	95.069 ^b	155.89 ^b	-	-	-
	297.9 ^c	95.8 ^c	154.4 ^c	-	-	-
MgS	153.47	39.75	53.58	168.4 ^d	42.2 ^d	55.2 ^d
MgSe	127.78	32.90	42.55	112.66 ^e	33.49 ^e	42.65 ^e
MgTe	100.58	24.88	29.99	94 ^f	24 ^f	29 ^f
CaO	230.72	58.90	77.14	198.8 ^g	57.1 ^g	75.3 ^g
	-	-	81 ^h	-	-	-
	220.53 ⁱ	57.67 ⁱ	80.03 ⁱ	-	-	-
CaS	139.88	23.27	34.05	122.1 ^g	23.9 ^g	33.5 ^g
CaSe	119.12	18.97	27.42	104.3 ^g	19.4 ^g	26.6 ^g
CaTe	94.34	13.92	18.70	94.13 ^j	13.76 ^j	17.34 ^j
SrO	186.69	48.25	55.15	159.7 ^k	46.7 ^k	54.3 ^k
	-	-	56 ^h	-	-	-
SrS	122.77	18.40	26.17	109.7 ^k	19.1 ^k	26.3 ^k
SrSe	106.57	14.63	21.33	93.6 ^k	15.2 ^k	21.1 ^k
SrTe	86.14	10.33	14.75	54.8 ^l	13 ^l	21 ^l
BaO	142.02	44.61	36.04	121.99 ^m	42.12 ^m	36.33 ^m
	-	-	34 ⁿ	-	-	-
BaS	104.74	16.60	18.58	91.29 ^m	16.7 ^m	18.74 ^m
BaSe	93.43	12.91	15.53	78.42 ^m	13.14 ^m	15.61 ^m
BaTe	78.04	8.56	11.09	68.36 ^m	9.1 ^m	11.26 ^m
PbTe	126.49	4.31	14.88	136.2 ^o , 102.93 ^p	3.79 ^o , 10.125 ^p	17.14 ^o , 12.641 ^p
	128.1 ^q	4.4 ^q	15.14 ^q	-	-	-

^aRef. ¹⁰ ^bRef. ¹¹ ^cRef. ¹² ⁱRef. ¹³ ^dRef. ¹⁴ ^eRef. ³ ^f Ref. ¹⁵ ^gRef. ¹⁶ ^hRef. ¹⁷ ^j Ref. ¹⁸ ^k Ref. ¹⁹

^lRef. ²⁰ ^mRef. ²¹ ⁿRef. ²² ^pRef. ²³ ^oRef. ²⁴ ^qRef. ²⁵

Table S3: Calculated Young's modulus (E, in GPa), Bulk modulus (B, in GPa), Shear modulus (G, in GPa), density (ρ , in gr/cc), sound velocities (v_l , v_t and v_m , in km/s), Debye temperature (Θ_D , in K), Poisson's ratio (σ) and Grüneisen parameter (γ) for MX compounds.

Compound	E	B	G	ρ	v_l	v_t	v_m	Θ_D	σ	γ
MgO	300.23	158.11	126.84	3.59	9.55	5.95	6.55	927.14	0.18	1.23
Others	305 ^a	165.5 ^a	127.9 ^a	3.0 ^a	9.826 ^a	6.115 ^a	6.740 ^a	902 ^a	0.252 ^a	-
MgS	133.23	77.66	54.87	2.70	7.47	4.51	4.98	573.55	0.21	1.24
Others	-	73.102 ^b 79.44 ^c 72.3 ^d	-	-	-	-	-	-	-	-
MgSe	108.43	64.52	44.44	4.25	5.40	3.23	3.58	391.45	0.22	1.36
Others	113.07 ^e 109.2 ^f	60.203 ^b 67.7 ^e 65.15 ^c	46.28 ^e 45.7 ^f	-	-	-	-	-	0.2216 ^e	-
MgTe	81.03	50.11	32.92	4.91	4.38	2.59	2.87	289.54	0.23	1.41
Others	77 ^g	45.795 ^b 50.45 ^c 44.6 ^d	31 ^g	-	4.420 ^g	2.243 ^g	-	251 ^g	0.33 ^g	-
CaO	196.26	116.17	80.54	3.42	8.09	4.85	5.37	669.61	0.22	1.36
Others	178.51 ^h 205.6 ^a	104.32 ^h 118.8 ^a	73.47 ^h 84.88 ^a	3.2 ^a	8.394 ^a	5.085 ^a	5.619 ^a	691 ^a	0.21 ^h 0.221 ^a	-
CaS	103.43	62.14	42.30	2.67	6.66	3.98	4.40	465.12	0.22	1.37
Others	95.27 ^h	56.62 ^h 62.90 ⁱ 64 ^j	39.06 ^h	-	-	-	-	-	0.22 ^h	-
CaSe	85.82	52.35	34.98	3.90	5.04	2.99	3.32	336.21	0.23	1.39
Others	78.69 ^h	47.70 ^h 52.17 ⁱ 51 ^j	32.12 ^h	-	-	-	-	-	0.23 ^h	-

^aRef. ¹⁰ ^bRef. ²⁶ ^cRef. ²⁷ ^dRef. ¹ ^eRef. ²⁸ ^fRef. ³ ^g15 ^hRef. ¹⁶ ⁱRef. ¹⁸ ^jRef. ²⁹ ^kRef. ³⁰

Table S3 continued

Compound	E	B	G	ρ	v_l	v_t	v_m	Θ_D	σ	γ
CaTe	63.39	40.73	25.55	4.46	4.10	2.40	2.65	251.08	0.24	1.45
Others	62 ^g	39.6 ^k 40.45 ⁱ 41.8 ^j	25 ^g	-	4.246 ^g	1.998 ^g	-	209 ^g	-	-
SrO	149.36	94.4	60.41	4.30	6.38	3.75	4.15	481.98	0.24	1.43
Others	135.81 ^l 139 ^a	82.4 ^l 87.6 ^a	55.13 ^l 56.28 ^a	4.9 ^a	5.743 ^a	3.385 ^a	3.751 ^a	430 ^a	0.23 ^l 0.222 ^a	-
SrS	85.36	53.19	34.63	3.72	5.17	3.05	3.38	336.80	0.23	1.42
Others	80.48 ^l	47.3 ^l	32.77 ^l	-	-	-	-	-	0.23 ^l	-
SrSe	72.04	45.28	29.17	4.63	4.26	2.51	2.78	266.98	0.23	1.43
Others	66.80 ^l	40.3 ^l	27.14 ^l	-	-	-	-	-	0.23 ^l	-
SrTe	54.24	35.6	21.77	4.94	3.62	2.10	2.33	209.78	0.25	1.48
Others	64.77 ^m	22.12 ^m 39.5 ⁿ	23.54 ^m	-	3.996 ^g	1.714 ^g	-	119.450 ^m 172 ^g	0.019 ^m 0.39 ^g	-
BaO	103.75	77.08	40.66	6.01	4.67	2.60	2.90	311.79	0.28	1.63
Others	107.45 ^o 106.2 ^a	76.3 ^a	41.88 ^a	5.7 ^a	4.76 ^a	2.672 ^a	2.973 ^a	316 ^a	0.35 ^o 0.255 ^a	-
BaS	66.63	45.98	26.47	4.37	4.31	2.46	2.74	256.14	0.26	1.54
Others	88.24 ^o	41.6 ^p	24.935 ^p	-	4.2 ^q	2.37 ^q	2.67 ^p 2.64 ^q	247.26 ^p 247 ^q	0.18 ^o 0.25 ^p	-
BaSe	57.85	39.75	23.00	5.05	3.73	2.13	2.38	214.81	0.26	1.53
Others	76.21 ^o ,	34.0 ^r 36.267 ^p	21.41 ^p	-	3.64 ^q	2.07 ^q	2.3 ^p 2.31 ^q	205.7 ^p 208 ^q	0.17 ^o 0.252 ^s 0.25 ^p	-
BaTe	45.17	31.72	17.89	5.20	3.27	1.85	2.06	176.28	0.26	1.56
Others	67.15 ^o	27.04 ^r 28.23 ^p	16.697 ^p	-	3.68 ^g	1.46 ^g	1.99 ^p	171.22 ^p 139 ^g	0.13 ^o 0.271 ^s 0.25 ^p	-
PbTe	68.24	45.04	27.35	8.32	3.13	1.81	2.01	186.07	0.25	1.50
Others	54.72 ^t	41.06 ^t	21.99 ^t	-	2.94 ^t	1.64 ^t	1.83 ^t	266.51 ^t	0.273 ^t	-

^aRef.¹⁰ ^g Ref.¹⁵ ^lRef.¹⁹ ^mRef.³¹ ⁿ Ref.³² ^o Ref.²¹ ^pRef.³³ ^qRef.³⁴ ^rRef.³⁵ ^sRef.³⁶ ^tRef.²³

References

- (1) Mir, S. H.; Jha, P. C.; Dabhi, S.; Jha, P. K. Ab initio study of phase stability, lattice dynamics and thermodynamic properties of magnesium chalcogenides. *Materials Chemistry and Physics* **2016**, *175*, 54–61.
- (2) Ghebouli, M.; Choutri, H.; Bouarissa, N. Electronic structure and lattice dynamics of $\text{Ca}_x\text{Mg}_{1-x}\text{S}$ in the rock-salt phase. *Materials Science in Semiconductor Processing* **2014**, *18*, 71–79.
- (3) Wu, H.; Chen, Y.; Deng, C.; Han, X.; Yin, P. Electronic, elastic and dynamical properties of MgSe under pressure: rocksalt and iron silicide phase. *Philosophical Magazine* **2015**, *95*, 2240–2256.
- (4) Ghebouli, M.; Choutri, H.; Bouarissa, N.; Ghebouli, B.; Fatmi, M.; Uçgun, E. Ab initio calculation of fundamental properties of $\text{Ca}_x\text{Mg}_{1-x}\text{A}$ (A = Se and Te) alloys in the rock-salt structure. *Physica E: Low-dimensional Systems and Nanostructures* **2013**, *49*, 83–91.
- (5) Galtier, M.; Montaner, A.; Vidal, G. Phonons Optiques de CaO, SrO, BaO Au Centre de la Zone de Brillouin à 300 et 17K. *Journal of Physics and Chemistry of Solids* **1972**, *33*, 2295–2302.
- (6) Kaneko, Y.; Morimoto, K.; Koda, T. Optical Properties of Alkaline-Earth Chalcogenides. I. Single Crystal Growth and Infrared Reflection Spectra Due to Optical Phonons. *Journal of the Physical Society of Japan* **1982**, *51*, 2247–2254.
- (7) Souadkia, M.; Bennecer, B.; Kalarasse, F. Ab initio lattice dynamics and thermodynamic properties of SrO under pressure. *Journal of Physics and Chemistry of Solids* **2012**, *73*, 129–135.

- (8) Rieder, K. H.; Migoni, R.; Renker, B. Lattice dynamics of strontium oxide. *Physical Review B* **1975**, *12*, 3374–3379.
- (9) Souadkia, M.; Bennecer, B.; Kalarasse, F. Elastic and lattice dynamical properties of ternary strontium chalcogenide alloys. *Materials Science in Semiconductor Processing* **2014**, *26*, 267–275.
- (10) Cinthia, A. J.; Priyanga, G. S.; Rajeswarapalanichamy, R.; Iyakutti, K. Structural, electronic and mechanical properties of alkaline earth metal oxides MO (M=Be, Mg, Ca, Sr, Ba). *Journal of Physics and Chemistry of Solids* **2015**, *79*, 23–42.
- (11) Anderson, O. L.; Andreatch, P. Pressure Derivatives of Elastic Constants of Single-Crystal MgO at 23° and -195.8°C. *Journal of the American Ceramic Society* **1966**, *49*, 404–409.
- (12) Sinogeikin, S. V.; Bass, J. D. Single-crystal elasticity of MgO at high pressure. *Physical Review B* **1999**, *59*, R14141–R14144.
- (13) Oda, H.; Anderson, O.; Isaak, D.; Suzuki, I. Measurement of elastic properties of single-crystal CaO up to 1200 K. *Physics and Chemistry of Minerals* **1992**, *19*.
- (14) Saib, S.; Bouarissa, N.; Rodríguez-Hernández, P.; Muñoz, A. Ab initio lattice dynamics and piezoelectric properties of MgS and MgSe alkaline earth chalcogenides. *The European Physical Journal B* **2009**, *73*, 185–193.
- (15) Ren, Y. First principles study of electronic, phonon and elastic properties of rock-salt-phase MTe (M = Mg, Ca, Sr, Ba). *Computational Condensed Matter* **2017**, *11*, 69–76.
- (16) Abdus Salam, M. M. Theoretical study of CaO, CaS and CaSe via first-principles calculations. *Results in Physics* **2018**, *10*, 934–945.
- (17) Son, P.; Bartels, R. CaO and SrO single crystal elastic constants and their pressure derivatives. *Journal of Physics and Chemistry of Solids* **1972**, *33*, 819–828.

- (18) Maizi, R.; Boudjahem, A.-G.; Boulbazine, M. First-Principles Investigations on Structural, Elastic, and Thermodynamic Properties of CaX (X = S, Se, and Te) under Pressure. *Russian Journal of Physical Chemistry A* **2019**, *93*, 2726–2734.
- (19) Salam, M. M. A. First principles study of structural, elastic and electronic structural properties of strontium chalcogenides. *Chinese Journal of Physics* **2019**, *57*, 418–434.
- (20) Varshney, D.; Jain, S.; Shriya, S.; Khenata, R. High-pressure and temperature-induced structural, elastic, and thermodynamical properties of strontium chalcogenides. *Journal of Theoretical and Applied Physics* **2016**, *10*, 163–193.
- (21) Kumar, P.; Rajput, K.; Roy, D. R. Structural, electronic, vibrational, mechanical and thermoelectric properties of 2D and bulk BaX (X=O, S, Se and Te) series under DFT and BTE framework. *Physica E: Low-dimensional Systems and Nanostructures* **2021**, *127*, 114523.
- (22) Vetter, V.; Bartels, R. BaO single crystal elastic constants and their temperature dependence. *Journal of Physics and Chemistry of Solids* **1973**, *34*, 1448–1449.
- (23) Xue, F.; Wang, J.; Liu, X.; Sun, X. Study of electronic structure, elastic properties and thermodynamic properties of three PbTe phases: First-principles calculations. *Optik* **2021**, *232*, 166533.
- (24) Yang, Y. L. Elastic moduli and band gap of PbTe under pressure:ab initiostudy. *Materials Science and Technology* **2012**, *28*, 1308–1313.
- (25) Dornhaus, R.; Nimtz, G.; Schlicht, B. *Narrow-Gap Semiconductors*; Springer Berlin Heidelberg, 1983.
- (26) Tairi, L.; Touam, S.; Boumaza, A.; Boukhtouta, M.; Meradji, H.; Ghemid, S.; Omran, S. B.; Hassan, F. E. H.; Khenata, R. Phase stability and electronic behavior of MgS, MgSe and MgTe compounds. *Phase Transitions* **2017**, *90*, 929–941.

- (27) Debnath, B.; Sarkar, U.; Debbarma, M.; Bhattacharjee, R.; Chattopadhyaya, S. Modification of band gaps and optoelectronic properties of binary calcium chalcogenides by means of doping of magnesium atom(s) in rock-salt phase- a first principle based theoretical initiative. *Journal of Solid State Chemistry* **2018**, *258*, 358–375.
- (28) Muthaiah, R.; Garg, J. Thermal conductivity of magnesium selenide (MgSe)–A first principles study. *Computational Materials Science* **2021**, *198*, 110679.
- (29) Luo, H.; Greene, R. G.; Ghandehari, K.; Li, T.; Ruoff, A. L. Structural phase transformations and the equations of state of calcium chalcogenides at high pressure. *Phys. Rev. B* **1994**, *50*, 16232–16237.
- (30) Charifi, Z.; Baaziz, H.; Hassan, F. E. H.; Bouarissa, N. High pressure study of structural and electronic properties of calcium chalcogenides. *Journal of Physics: Condensed Matter* **2005**, *17*, 4083–4092.
- (31) Saoud, F. S.; Rabah, K.; Bouhemadou, A.; Plenet, J. C.; Henini, M.; Djabou, R. E. H. Structural Stabilities and Elastic Thermodynamic Properties of SrTe Compound and SrTe_{1-x}Ca_x Alloy Under High Pressure. *Journal of Electronic Materials* **2016**, *46*, 766–774.
- (32) Zimmer, H. G.; Winzen, H.; Syassen, K. High-pressure phase transitions in CaTe and SrTe. *Phys. Rev. B* **1985**, *32*, 4066–4070.
- (33) Musari, A. A.; Orukombo, S. A. Theoretical study of phonon dispersion, elastic, mechanical and thermodynamic properties of barium chalcogenides. *International Journal of Modern Physics B* **2018**, *32*, 1850092.
- (34) Gökoğlu, G. First principles study of barium chalcogenides. *Journal of Physics and Chemistry of Solids* **2008**, *69*, 2924–2927.

- (35) Drablia, S.; Boukhris, N.; Boulechfar, R.; Meradji, H.; Ghemid, S.; Ahmed, R.; Omran, S. B.; Hassan, F. E. H.; Khenata, R. Ab initio calculations of the structural, electronic, thermodynamic and thermal properties of $\text{BaSe}_{1-x}\text{Te}_x$ alloys. **2017**, *92*, 105701.
- (36) Khalfallah, B.; Driss-Khodja, F.-Z.; Saadaoui, F.; Driss-Khodja, M.; Boudali, A.; Bendaoud, H.; Bouhafs, B. A first-principles study of the structural, elastic, electronic, vibrational, and optical properties of $\text{BaSe}_{1-x}\text{Te}_x$. *Journal of Computational Electronics* **2018**, *17*, 1478–1491.